

Fabrication, Characterization, and Kinetic Study of Cu-MOF hybrids as electrocatalyst for Hydrogen Evolution Reaction



By

Abdul Shakoor Sabir

**School of Chemical and Materials Engineering
National University of Sciences and Technology**

2022

Fabrication, Characterization, and Kinetic Study of Cu-MOF hybrids as electrocatalyst for Hydrogen Evolution Reaction



Name: Abdul Shakoor Sabir

Registration No: 00000328653

**This thesis is submitted as a partial fulfilment of the requirements
for the degree of**

MS in Chemical Engineering

Supervisor Name: Dr. Erum Pervaiz

School of Chemical and Materials Engineering (SCME)

National University of Science and Technology (NUST)

H-12, Islamabad, Pakistan

May, 2023



THESIS ACCEPTANCE CERTIFICATE

Certified that final copy of MS thesis written by Mr Abdul Shakoor Sabir (Registration No 00000328653), of School of Chemical & Materials Engineering (SCME) has been vetted by undersigned, found complete in all respects as per NUST Statues/Regulations, is free of plagiarism, errors, and mistakes and is accepted as partial fulfillment for award of MS degree. It is further certified that necessary amendments as pointed out by GEC members of the scholar have also been incorporated in the said thesis.

Signature: SB

Name of Supervisor: Dr Erum Pervaiz

Date: 24/7/23

Signature (HOD): SB

Date: 24/7/23

Signature (Dean/Principal): AA

Date: 26.7.23



Form TH-1
(Must be type written)

National University of Sciences & Technology (NUST)
MASTER'S THESIS WORK
Formulation of Guidance and Examination Committee (GEC)

Name: Abdul Shakoor Sabir

NUST Reg No: 00000328653

Department: Chemical Engineering (SCME)

Specialization: Chemical Engineering

Credit Hour Completed: 20 24

CGPA: 3.67 3.69

Course Work Completed

S/No	Code	Title	Core/Elective	CH	Grade
1	EME 921	Momentum Heat and Mass Transfer	Core	03	A
2	CHE 843	Separation Processes in Chemical Engineering	Core	03	A
3	CHE-853	Green Process Engineering	Elective	03	B+
4	RM 898	Research Methodology	Elective	02	Q
5	CHE-847	Chemical Kinetics & reactor design	Core	03	B+
6	CHE-814	Product Technology	Elective	03	A
7	ESE-826	Industrial Catalysis for energy Application	Elective	03	B

*

Date: 22-10-21

Student's Signature: [Signature]

Thesis Committee

- Name: Dr. Erum Pervaiz (Supervisor)
Department: Chemical Engineering
- Name: Dr. Umair Sikandar
Department: Chemical Engineering
- Name: Dr. Amm Shahid
Department: Chemical Engineering

Signature: [Signature]

Signature: [Signature]

Signature: [Signature]

Date: 22/10/21

Signature of Head of Department: [Signature]

APPROVAL

Date: 25-10-21

Signature of Dean/Principal: [Signature]

Distribution

1x copy to Exam Branch, Main Office NUST

1x copy to PGP Dte, Main Office NUST

1x copy to Exam branch, respective institute

School of Chemical and Materials Engineering (SCME) Sector H-12, Islamabad

8. CHE-848 Crasification Processes Elective 3.0 A
9. ESE-911 Carbon capture & Utilization Elective 3.0 B+



Form: TH-04

National University of Sciences & Technology (NUST)

MASTER'S THESIS WORK

We hereby recommend that the dissertation prepared under our supervision by
Regn No & Name: 00000328653 Abdul Shakoor Sabir

Title: Fabrication, Characterization and Kinetic Study of Cu-MOF Hybrids as Electrocatalyst for Hydrogen Evolution Reaction.

Presented on: 06 Jul 2023 at: 1400 hrs in SCME Seminar Hall

Be accepted in partial fulfillment of the requirements for the award of Master of Science degree
in Chemical Engineering.

Guidance & Examination Committee Members

Name: Dr Ameen Shahid

Signature: [Signature]

Name: Dr Umair Sikandar

Signature: [Signature]

Supervisor's Name: Dr Erum Pervaiz

Signature: [Signature]

Dated: 10/7/23

[Signature]
Head of Department
Date 10/7/23

[Signature]
Dean/Principal
Date 12.7.2023

School of Chemical & Materials Engineering (SCME)

Dedication

By the grace of Almighty Allah, who is the Most Beneficent and
the Most Merciful

This study is dedicated to my parents, who have always been my
source of guidance and support.

To my supervisor who shared her knowledge, gave advice, and
encouraged me to fulfill my objectives.

And to all my fellows I worked with whom I've enjoyed
wonderful memories.

Acknowledgements

The fact that we can reason and that we have the desire to learn more about the universe are both gifts from Allah. Everything and anything in this universe require the will of Allah, the Almighty. Sincere greetings to the Holy Prophet Muhammad (PBUH), whom I consider to be the origin of the cosmos as well as an unending source of knowledge and a blessing for all of humanity.

The illustrious Dr. Erum Pervaiz, who was my supervisor, deserves appreciation for having faith in me. Her consistent direction, inspiration, and backing were all extremely important to the success of the project. The help that was provided by the NUST Pakistan research facilities as well as the HEC project designated (2017/HEC/NRPU-10482) is greatly appreciated by the author, Erum Pervaiz.

I'd want to use this opportunity to extend my most heartfelt gratitude to my GEC members Dr. Umair Sikandar, and Dr. Ameen Shahid. On the other hand, I am thankful for the support of people who are closest to me and will always be there for me, regardless of how challenging things become. My heartfelt appreciation goes out to everyone who has helped me in SCME and in the laboratory. Thank you!

Abdul Shakoor Sabir

Abstract

To satisfy the ever-increasing need for energy around the world, science is currently confronted with its greatest challenge. Most of the world's electricity is still produced by burning fossil fuels such as oil, coal, and natural gas. This is the case even though renewable sources of energy are becoming more and more popular. During the entire process of converting hydrogen into electricity, it only produces heat and water, making it an environmentally friendly fuel source. Water splitting is one of the renewable sources to produce hydrogen but requires a catalyst to minimize the potential to break water molecules. The economic viability of water splitting to produce hydrogen (H₂) is constrained by the reaction's unfavorable kinetics. The development of catalytically active and structurally stable electrocatalysts is challenging despite high demand. In many cases, a catalyst is necessary for electrocatalytic water splitting. Long-term stability and high catalytic activity are two of the biggest obstacles to overcome when developing a catalyst for the hydrogen evolution process (HER). The process of decomposing water into its parts, hydrogen, and oxygen, holds great potential. Using inexpensive water-splitting equipment and electrolyzer, it may be possible to manufacture marketable H₂ fuel. It is necessary to consider several different parameters to develop an electrocatalyst for the hydrogen evolution reaction (HER) that is both cost-effective and highly active for the process of water splitting. In this experiment, the metal-organic framework formed from Cu-BTC and g-C₃N₄ is joined to form a hybrid catalyst, which is then synthesized using a solvothermal method. The Tafel slope of 59 mV/dec in 1 M KOH electrolyte and the low overpotential (only 131 mV at 10 mA/cm²) are just two of the remarkable characteristics of the Cu-BTC/g-C₃N₄ catalyst that was built for HER electrocatalysis. Other remarkable characteristics include. This one performs just as well as, or even better than, its predecessors when measured against the performance of other Cu-BTC hybrids. According to the findings, using Cu-BTC hybrids as an electrocatalyst for hydrogen evolution has the potential to be beneficial.

Table of Contents

Dedication.....	i
Acknowledgements.....	ii
Abstract.....	iii
List of Figures.....	vii
List of Tables	viii
Acronym	ix
Chapter 1	1
Introduction	1
1.1 Background.....	1
1.2 Essentials of Water Splitting.....	3
1.3. Kinetics of Hydrogen Evolution Reaction and Oxygen Evolution Reaction	6
1.6 Problem Statement.....	8
1.7 Research Objective	9
1.8 Scope of Study	9
1.9 Chapter Summary	9
Chapter 2	11
Literature Review	11
2.1 Literature Review	11

2.2 Cu-BTC and its synthesis Methods	12
2.2.1 Applications of MOF catalysts for Water Splitting	14
2.3. Cu-Based Catalysts for Water Splitting.....	16
2.3.1. Cu-Based layered double hydroxides for OER and HER	19
2.3.2. Cu-Based phosphides for OER and HER.....	25
2.3.3 Ru-modified Cu-BTC.....	29
2.3.4. Channel-rich RuCu nanosheets	30
2.3.5 Ru-doped Cu electrocatalysts	30
2.3.6 AB & Cu-MOF composite	31
Chapter 3	32
Materials and Methods	32
3.1 Chemicals and reagents	32
3.2 Preparation of Pure Cu-BTC.....	32
3.3 Preparation of Pure g-C ₃ N ₄	32
3.4 Preparation of Hybrids Cu-BTC/ g-C ₃ N ₄	32
3.5 Characterization and Electrochemical Study	33
Chapter 4	34
Result and Discussion.....	34
4.1 X-ray diffraction (XRD).....	34

4.2 Scanning Electron Microscopy (SEM) and Energy Dispersive X-Ray (EDX)	36
4.4 Electrochemical study	38
4.4.1 Hydrogen Evolution Reaction (HER) and Oxygen Evolution Reaction (OER)	38
4.4.2 Cyclic Voltammetry (CV) and Electrochemical Impedance Spectroscopy (EIS)	40
4.4.3 Chronopotentiometry	42
Conclusions	44
Recommendation	45
References	46

List of Figures

Figure 1: Illustration of photocatalysis process over semiconductors [64].....	4
Figure 2 a) Two different HER mechanisms of catalysts in acidic electrolytes[85]	8
Figure 3 Classification of MOFs [112].....	12
Figure 4 (Analysis of Cu-LMM [151].....	17
Figure 5 Analysis of Cu-LSM for HER, OER, and Stability [152].....	18
Figure 6 (a) LSV and (b) Co ₃ O ₄ , CuO, and Co ₃ O ₄ –CuO nano-based composites taffel slopes (reproduced with permission from Elsevier, copyright 2019) [153].....	19
Figure 7 (LSV, efficiency, Resistance plot, GSTAT, and structure) [154].....	22
Figure 8 (Analysis of the Cu-Co-Fd-DH) [155].....	23
Figure 9 Preparation of NiCu phosphide over NF for HER reaction (reproduced with permission from ACS publications, copyright 2017) [161]	27
Figure 10 (a-d) LSV, Cu ₃ P catalysts in KOH for two-electrodes, the scheme, and PSTAT analysis for 12 h (reproduced with permission) [161]	28
Figure 11 XRD of the prepared samples.	35
Figure 12: SEM images of Pure Cu-BTC, and hybrid samples	37
Figure 13: (a) EDS of pure Cu-BTC, (b) EDS of the hybrid having 15 mg of Cu-BTC/g-C ₃ N ₄	37
Figure 14: (a, b) HER and OER of the prepared samples, (c,d) Tafel slopes of HER and OER of the prepared samples respectively.....	40
Figure 15: (a) CV curves of all the catalysts, (b) EIS of the prepared Catalysts.....	41
Figure 16: Chrono of the catalyst for 18 h	43

List of Tables

Table 1: MOF-based catalysts performance Summary	16
Table 2: Average crystal sizes of the prepared samples.....	35
Table 3: EIS summary of Prepared Catalysts	42

Acronym

OER:	Oxygen evolution reaction
HER:	Hydrogen evolution reaction
ECSA:	Electrochemical active surface area
MOF:	Metallic Organic framework
SEM:	Scanning Electron Microscope
EDX:	Energy-dispersive X-ray spectroscopy
XRD:	X-ray diffraction
dec⁻¹:	Decade
Pt:	Platinum
CV:	Cyclic Voltammetry
LSV:	Linear cyclic voltammetry
EIS:	Electrochemical Impedance Spectroscopy

Chapter 1

Introduction

1.1 Background

The greatest difficulty that the present scientific age has is meeting the enormous demand for energy that the modern era has created. Even while the need for energy around the globe is growing, most of the world's electricity is still generated by the combustion of fossil fuels like oil, natural gas and coal [1], [2], [3]. Scientists are turning their focus to clean, renewable energy sources and devoting more resources to them when nonrenewable energy sources are depleted, and attempts are made to minimize pollution. This move comes as scientists are also making progress in reducing pollution. Hydrogen has the potential to grow into a substantial energy source in the not-too-distant future [4]–[7]. This is because it generates a significant quantity of energy from non-depletable, renewable resources like water and the energy of light (photons)[8], [9]. This potentially renewable fuel is utilized in a wide variety of vehicles, including airplanes, electrical devices, and even spacecraft. It is not possible to extract individual hydrogen molecules because these subatomic particles are an inseparable component of all organic matter, including water and hydrocarbons. Alternative methods include bio-photolysis, dark fermentation, photo-fermentation, integrated fermentation, and artificial photosynthesis [10]–[13]. Viable choices include hydrocarbon steam reforming, non-catalytic partial oxidation, electrolysis of water, and auto-thermal reforming. Even though there are various other techniques, up to 98% of all hydrogen produced is still derived from fossil fuels. Natural gas makes up 40% of the total, oil makes up 30%, coal makes up 18%, water electrolysis makes up 4%, and biomass can make up as much as 1% of the total[14]–[17].

The development of approaches for the large-scale generation of hydrogen will make it possible to extract hydrogen from substances that already contain hydrogen on their own. The production of hydrogen can be divided into two categories: those that concentrate on the material from which hydrogen is extracted and those that concentrate on the energy source that drives the extraction process[18], [19], [20]. The electrochemical water splitting takes input energy of $G = 237.1 \text{ kJ mol}^{-1}$, which is equivalent to a thermodynamic

potential of 1.23 V when performed under ordinary conditions[21]–[24]. HER and OER have relatively low energy conversion efficiencies because they require significant overpotentials to achieve substantial current densities. This is the reason why these reactions have relatively low energy conversion efficiencies[25], [26]. Due to this, the potential required for water splitting is higher than 1.23 in the working electrochemical setup[27].

Despite the many investigations that have been carried out over the past ten years[28], the noble metal-based catalysts (platinum for acidic water electrolysis and iridium or ruthenium oxides for alkaline water electrolysis) continue to be the most effective. Metal-organic frameworks, often known as MOFs, are a newly discovered family of materials that, despite their great porosity, exhibit exceptional crystallinity and long-range organization [29]. MOFs are constructed from organic ligands and metal ions (or clusters), which serve as the basic elements. MOFs have clusters of metal or ions of metal along with solvent molecules and organic ligands. During MOF-driven catalytic processes, the coordinated solvent molecules, such as water, frequently become unstable. Because of this, the metal center of the MOF will be coordinatively unsaturated[30], [31]. The dynamic structure, ultrahigh surface area, design tunability, and crystalline nature of the material, in addition to its high porosity (90% free volume), contribute to the remarkable optical, electrical, and catalytic properties that come from the material. Their possible applications have lately been researched in a variety of various domains, including carbon dioxide (CO₂) collection, sensing, adsorption, and catalysis[32]–[34]. MOFs have been the subject of extensive research due to the possibility that they could operate as an active catalyst in the electrochemical and photoelectrochemical (PEC) generation of hydrogen[33], [35]–[37]. Cu-based MOFs offer high stability, electrochemical properties, photochemical properties, high catalytic activity, and stability and due to this, it has been the subject of research for a variety of applications. Some of these applications include hydrogen storage, photovoltaics, ammonia sensing, HER, and absorption, CO₂ reduction[38]–[42].

Based on the Cu-Pd findings, the overpotential was determined to be 200 mV, and the Tafel slope was determined to be 28.2 Vdec⁻¹[43]. Ting Song and colleagues demonstrated that hydrogen evolution might be accelerated by using photocatalysis using visible light

in their experiment. The Cu-based MOF demonstrates a variety of desirable characteristics, including a high hydrogen evolution rate (5.7 mmolh^{-1}) and outstanding long-term stability when irradiated with visible light[44]. Meso-Cu-BTC MOF electrocatalyst was prepared with minimal effort using a basic method in alkaline media and had a low overpotential (89.32 mV), onset potential (25 mV), and Tafel slope (33.41 mVdec^{-1}) [42].

1.2 Essentials of Water Splitting

Photocatalysis and electrocatalysis are two methods that can be used to split water molecules[45], [46]. These methodologies have the potential to produce hydrogen in the most effective and environmentally friendly manner. It takes a large amount of time to create an O-O bond, which results in the loss of four electrons and four protons, making it a significant bottleneck in the process of splitting water[47].

1.2.1. Photocatalytic Water Splitting

As demonstrated in Figure 1a, water can be broken down into its parts, hydrogen, and oxygen, by utilizing photocatalysts. The process of photocatalysis on semiconductor particles can be broken down into three primary stages: i) the photon absorption having high energy compared to the semiconductor bandgap, which leads to the hole pair and electron generation in the semiconductor particles; (ii) separation of charges, and shifting of photogenerated carriers in the particles; and (iii) the chemical reaction occurs at the surface between semiconductor particles and photogenerated carriers (for example, H_2O) [48], [49], [50]. Criteria for photocatalysts are: (i) have a larger charge separation, (ii) have faster charge transportation, and (iii) have a narrow energy gap between their bandgap and band edge[51].

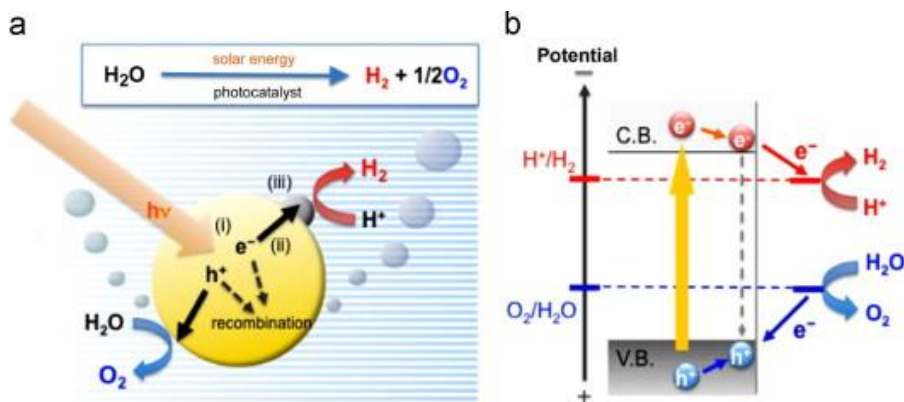


Figure 1: Illustration of photocatalysis process over semiconductors [52]

To make the process of H₂ evolution easier, thin layers of semiconductor materials that can be employed for photocatalysis and electrocatalysis is prepared. Different catalysts have been produced for photocatalysis of water splitting i.e., FTO, When analyzing water splitting in the visible spectrum, mesoporous titania thin films produced on fluorine-doped tin oxide (FTO) electrodes were used[53]–[56]. However, other typical semiconductors such as silicon carbide (SiC), zinc oxide (ZnO), and cadmium sulfides (CdS) are inactive for the process of water splitting. This is because the band gaps of these materials do not align well with the redox potential required for this process, which results in photo deterioration. In the process of photo-corrosion, photogenerated holes take the place of water as the oxidant of the anion in the catalyst. In addition, most semiconductor catalysts require ultraviolet (UV) radiation, even though only around 4% of the energy that the sun provides is UV[57]. Because visible light makes up more than half of all incoming solar energy, researchers are actively looking for photocatalysts that work well in the visible light spectrum. This is because these photocatalysts have the potential to increase the efficiency with which solar power is generated. For the band gap of semiconductor materials to be sensitive to visible light, the value of the band gap must be less than 3eV[58]. Semiconductor catalysts that are combined with carbon materials or precious metal particles have been found to produce a superior response to visible light[59]. In visible light photocatalytic water splitting, metal sulfides, metal nitrides, and metal-free catalysts are all viable options[60].

1.2.2. Electrocatalytic Water Splitting

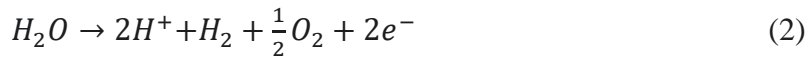
The hydrogen production takes place at the cathode of an electrochemical water split, whereas the production of oxygen takes place at the anode. The theoretical minimum voltage needed to split water is 1.23 V ($G = 237.2 \text{ kJ mol}^{-1}$), as per the equation[61], [62]. However, because of kinetics, additional voltage is required on both the cathode and the anode to initiate the reactions. A significant amount of work has been put into inventing outstanding catalysts to reduce the overpotential for complete water splitting. Even though the HER process works best in acidic solutions, full water splitting with non-noble metal catalysts can typically only be achieved in alkaline electrolytes[63] During the water splitting given below reaction occurs in acidic and basic electrolytic media[64]:

In acidic solution

Reaction at the cathode is:



Reaction at the anode is:



In neutral solution

Reaction at the cathode is:



Reaction at the anode is:

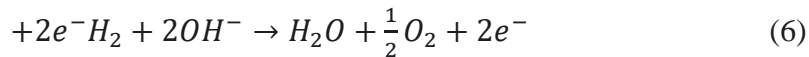


In alkaline solution

Reaction at the cathode is:



Reaction at the anode is:



Iridium and ruthenium-based materials for the OER and Pt composites for the HER are the most modern catalysts for splitting water in acidic media[65]. Because of the high price and restricted availability of the necessary materials, widespread application is impractical[29], [66]. These catalysts do not require the use of noble metals. There is reason to be optimistic about the catalytic performances of transition metal alloys, nitrides, sulfides, carbides, phosphides, and selenides in the HER [67]. To improve the catalytic activity of underlying catalysts in the process of water splitting, several different ways have been tried. These include manipulating the particle size, shape, dimensionality, composition, and the insertion of defects[68], as well as utilizing external excitation from light, magnetism, or electric field. Other methods include adjusting the structure of the interface between the two materials[69].

1.3. Kinetics of Hydrogen Evolution Reaction and Oxygen Evolution Reaction

Figure 2a illustrates the functional mechanism of the HER as a process that involves the transfer of two electrons[70]. The Volmer reaction, which includes the release of hydronium ions onto an electrode and ultimately results in the creation of hydrogen intermediates (H^*), is what kicks off the HER in an acidic electrolyte. When it comes to alkaline electrolytes, the water molecule itself acts as the proton donor[71]. The production of molecular hydrogen then occurs via two distinct pathways, both of which are dependent on the quantity of H^* surface coverage that is present. The rate-limiting step will be Tafel slope when there will be a large quantity of H^* atoms will be present. This is because two neighboring H^* can combine to generate H_2 molecules. Due to the ability to attract proton and electron at the same time in acidic conditions and attracting ability of molecules of water and electrons in alkaline media by H^* atoms, the Heyrovsky reaction will predominate if there will be low coverage of H^* [72].

Theoretically, the process of splitting water can begin when the thermodynamic potential reaches 1.23 V. The applicability of the HER is severely limited due to its poor kinetics

and huge overpotential [73]. To enhance the functionality of HERs and raise their level of efficiency, new and superior catalysts need to be created. Electrocatalysts based on noble metals continue to be the most successful kind of HER catalysts, despite the extensive research that has been done into alternative methods. To be more explicit, the following are requirements that must be met by any electrocatalytic material before it can be utilized in the HER: There is a high level of activity, long-term stability, low level of overpotential, low cost, and scalability potential for mass production[74].

Platinum (Pt), a particularly uncommon noble metal, is normally the one that is utilized in the role of primary catalyst for HER[75]. The high cost of these metals have a negative impact on their commercial value[76]. One of the most important strategies that have been devised is to replace an expensive metal electrocatalyst with an electrocatalyst made of a less expensive material[77]. Nonprecious carbides, sulfides, selenides, nitrides, phosphides, and oxides based on transition metals (such as cobalt, iron, molybdenum, nickel, and tungsten) have garnered a lot of interest because of their promising electrocatalytic activity[78]–[83]. This is because these nonprecious materials can be used to produce electrocatalysts. Earth-abundant metal electrocatalysts for HER have received considerable attention as a possible solution to these problems since they promise to be highly efficient, affordable, abundant, and long-lasting[84].

Platinum-group metals (PGM) are widely acknowledged as a benchmark for cathode catalysts across a broad pH range. This is mostly because of the high activity that these metals exhibit toward the HER[85]. The activity pattern of (111), (100), and (001) on the low-index, single-crystal faces of Pt have a major influence on the HER activity of the metal (110)[86]. For this process to occur, it is necessary to have reactive H_{opd} , which is normally found near the surface. This would imply that the surface of the Pt atom is noticeably more active than those of the other two[87].

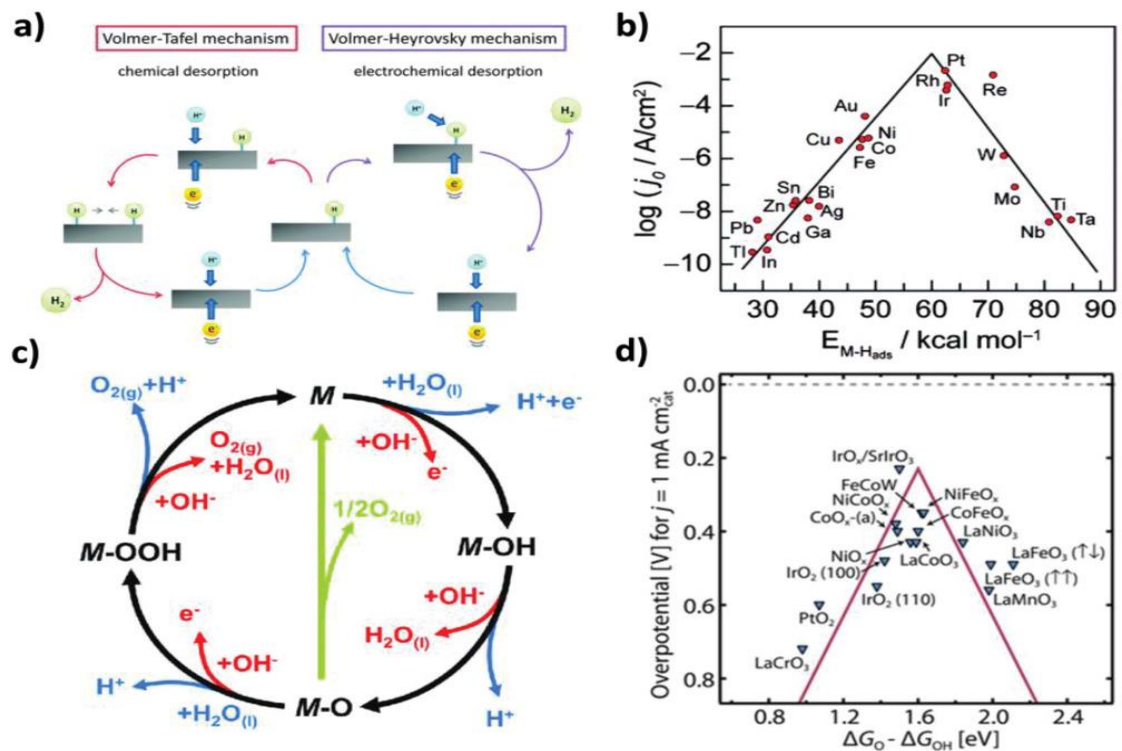


Figure 2 a) Two different HER mechanisms of catalysts in acidic electrolytes[71] .

Electrocatalysts were created by applying a 10 mA/cm^2 of current density and the resulting electrocatalysts exhibited overpotentials for HER that were lower than those of any phosphide-based composites that had been reported before[88]

1.6 Problem Statement

There is a direct correlation between the expansion of the world's population and the accompanying rise in the need for energy. For a significant amount of time, the burning of fossil fuels like natural gas and oil was the only method that could fulfill this requirement. Hydrogen, on the other hand, offers an alternative that is free of pollutants and is environmentally friendly once these resources run out. The molecules of water can be broken apart to make hydrogen, or methane can be reformed into hydrogen by the catalytic action of water. These are only two of the many ways that hydrogen can be produced. Utilizing a catalyst during the process of water splitting produces hydrogen as a byproduct. In the past, noble metals like Pt were employed as catalysts for this purpose. However, because noble metals are becoming scarcer and more expensive, a synthetic

catalyst that can speed up the process at a lower cost is necessary. The development of a catalyst for the generation of hydrogen gas through the application of Cu-BTC/g-C₃N₄ hybrids is the focus of this line of investigation. To conduct this experiment, electrolysis will be used, which is a process that separates hydrogen and oxygen from water.

1.7 Research Objective

The research objective is as follows:

- Preparation and analysis of Cu-BTC/g-C₃N₄ hybrid catalysts with different weight ratios of g-C₃N₄ material
- Analysis of overpotentials of Cu-BTC/g-C₃N₄ hybrid materials
- Analysis of applications of Cu-BTC/g-C₃N₄ hybrid catalysts for HER, and OER

1.8 Scope of Study

Pakistan is a growing country that doesn't have a lot of energy resources, so making hydrogen will make up for that. Hydrogen can be used as a fuel, to make energy, and in a lot of other ways.

- Making hydrogen over and over again is one of the best things about this process. Since water is used, which is the most common thing in nature, there is no chance that water will run out. Also, using transition metals as catalysts will cut down on the use of valuable rare metals and keep them from running out.
- By splitting water, hydrogen can be obtained, which can be used as a home fuel, in cars, and as a starting point for making many chemicals, like ammonia.

1.9 Chapter Summary

In total, there are five sections. The following chapters provide overviews of those parts.

- **Chapter 1** introduces the reader to the topic at hand, its historical background, and the problems that have surfaced as a direct result of this investigation. The topic, research objectives, and study parameters are all defined.
- **Chapter 2** will cover the literature review and previous efforts in the field of Cu-BTC hybrid synthesis, traditional method technique, water splitting, and its

aspects. There's also a look at how Cu-BTC and other hybrid building blocks compare as electrocatalysts.

- **Chapter 3** will cover the methods for creating hybrids, as well as pure Cu-BTC and g-C₃N₄.
- **Chapter 4** goes into greater detail regarding the results and analyses. Crystal structure and morphology of synthesized catalysts were characterized by XRD and SEM. This chapter also provides in-depth discussions of the electrochemical studies of active catalysts and their stability.
- **Chapter 5** synthesizes the findings of the investigation and makes recommendations for future study.

Chapter 2

Literature Review

2.1 Literature Review

Metal-organic frameworks, also known as MOFs, are porous crystalline solids with infinite lattices[89], [90]. These solids are known as metal-organic frameworks (MOFs)[91], [92]. In the 1990s, research groups led by Robson et al., Moore et al., Yaghi et al., Kitagawa et al., and Férey et al. laid the groundwork for MOF constructions and applications [93]. More than 20,000 different MOF structures have been identified, and because of BASF's efforts in mass production, many of these structures are now readily available for purchase via a variety of distributors, including These materials find use in a variety of industries, including oleo-chemicals, textiles, transportation, electric vehicle prototypes, food packaging, respiration systems, and chemical sensing[94].

The conductivity of metal-organic frameworks (MOFs) can be improved by combining them with other nanostructures like nanotubes and graphene. Graphene and nanotubes are examples of nanostructures that can be combined with MOFs to improve conductivity as can be seen in figure 3.

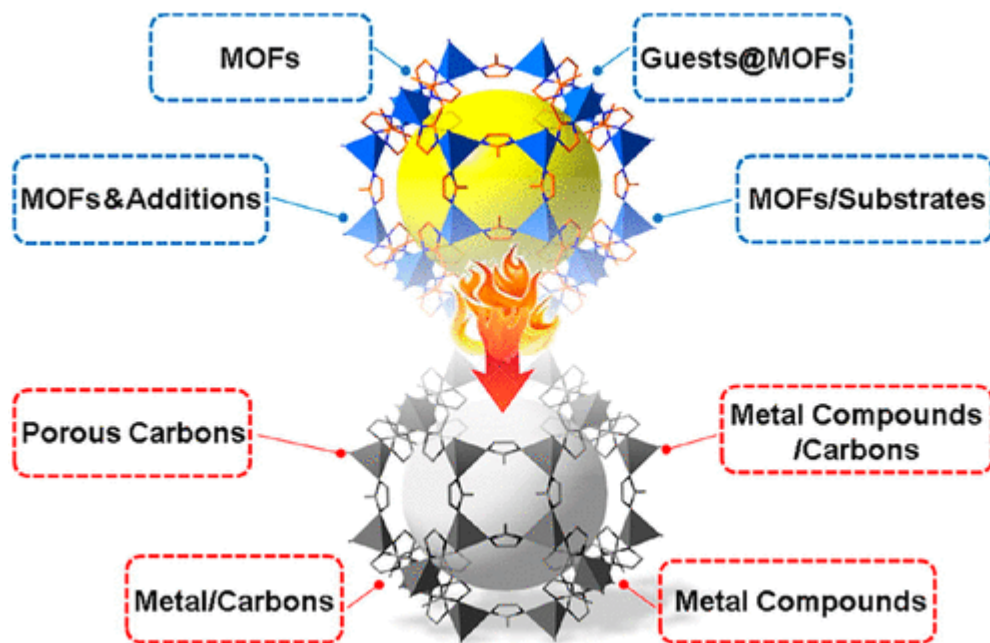


Figure 3 Classification of MOFs [93]

2.2 Cu-BTC and its synthesis Methods

The methods of synthesis for MOFs are divided into two types which include the modern and the conventional method. Sol-gel, Electrochemical, and solvothermal also known as hydrothermal are known as the conventional methods. Although MOFs are synthesized by some modern techniques which include microwave, sonication, evaporation, and spray drying[95]. Then, the solvent is used for washing the crystals obtained from the reaction carried out in the autoclave reactor. Water and ethanol are most used for washing. In solvothermal technique, organic nature solvents are used i.e., N, N-Dimethyl formaldehyde, and methanol [96].

Problems associated with solvent processes are their hazardous nature and disposal methods. The temperature range of the solvothermal process is 340-473K for the heating of the autoclave reactor and 2-6 days are average processing time. By the Solvothermal method, well-defined crystal structure, crystal size, and pore size are obtained. High requirements of energy and pressure, and processing in an autoclave reactor are bottlenecks for the solvothermal process. Mechanical method is also being used for the

synthesis and obtaining particular configurations of the MOFs crystals [96]. In the mechanical method, the reagent is stirred for a specified time in the beaker. After stirring, a filtration process is used for obtaining MOFs from solvents and then the sample is dried in a vacuum oven. In the Mechanical process, the temperature and time required are comparably lower than in the solvothermal method.

Sono-chemical employs sound frequencies for the synthesis of MOFs from their respective reagents [97]. In this method, the remaining suspensions are filtered out to obtain the fully developed MOFs crystals. The ultrasonication method is the most desired sono-chemical method as it increases the temperature at an exponential rate which is necessary for MOFs synthesis and the time required for the ultrasonication method is in the range of 1 hour [98]. The salient feature of this method is the high reaction rate and kinetics of the process [99]. These approaches are termed electrochemical methods for the synthesis of MOFs. Low pore volume and low surface area are major concerns for the Ultrasonication method.

Spray drying is a method in which no external forces are employed to bring the desired product [100]. The long period to yield is the major downside of this method[101], [102]. The chemical flow method is the other method in which no external forces are used, and, in these techniques, reagents are left in a beaker to react completely. The time of synthesis depends upon the completion of the reaction time. The temperature range of the Spray drying process is 302K- 573K. Synthesis by microwave is another method in which reagent is placed in the microwave radiator where reagents react under the energy obtained from the radiations[103], [104].

Table 1. provides a comparative study of various approaches used for the production of MOFs, in which the solvothermal method comes out to be the most efficient method as it offers excellent morphology and high crystallinity. According to the literature, the Solvothermal method is the least energy-intensive method comparing electrochemical, microwave, and sonochemical synthesis methods of MOFs. The solvothermal method also provides high pore volume and surface area comparing other synthesis methods. The major drawback associated with the solvothermal method is its reaction time as it takes 2-6 days to complete the synthesis process comparing other techniques. This compromises

the mass production of MOFs on an industrial scale [105]. Comparative Studies shows that the combination of solvothermal and microwave synthesis process offers high yield and low processing time. The major challenges involved in MOFs synthesis are: 1. high cost of synthesis. 2 low yields at industrial scale. 3. Highly energy intensive

2.2.1 Applications of MOF catalysts for Water Splitting

The ubiquitous application for MOFs in electrochemical water splitting can be attributed to their high surface areas, adaptable chemical components, configurable pore layouts, and diverse topologies[106], [107]. By coupling materials such as polyoxometalates (POMs), metallic compounds, CNTs, and other conductive substrates as guests @ MOFs or MOF/substrates, it is possible to adapt or modify the characteristics of MOFs[108]. By expanding the number of active sites and the conductivity of the material by a process called functionalization, one can achieve improved electrochemical performance in the procedure of water splitting[109].

The metal-organic framework can be utilized in its pure state[110]. When developing pure For HER, MOFs can focus their attention largely on the framework configuration as well as the catalytic activity. However it has only been utilized as an electrocatalyst for HER catalysis on a very infrequent basis. To solve the conductivity and instability issue, a great number of methods have been developed to improve the catalytic activity of untreated MOFs in the hydrogen evolution reaction[111].

A solvothermal approach was taken by Jayaram ulu et al. to produce nitrogen-doped graphene oxide and nickel sulfides (Ni₇S₆). After being chelated with oxygen and nitrogen, the Ni(II) metal centers of the NGO/Ni₇S₆ nano porous composite demonstrated improved for OER and HER. The huge number of pores, high surface area, and availability of nickel at the reaction interface contributed to an increase in the rate of gas release and mass transfer. During the process of optimizing the level of N-doping, the composite's stability was evaluated, and it was shown to be superior to that of the more prevalent RuO₂ and IrO₂ in OER settings. In another study based on graphene composites, ultrathin layers of graphene were used to encase nickel nanoparticles in metal (created from Ni-based MOF using a thermal process in an inert atmosphere). Research has demonstrated that a

carbon composite with Co-N doping produced have good performance level and a long lifespan for HER[112].

During the most recent few years, a great number of materials based on Co-MOF have been developed and implemented on a large scale as electrocatalysts for HER. Liu and colleagues developed Co/NBC by carbonizing cobalt-based boron imidazolate frameworks (BIF-82-Co) at varying pyrolysis temperatures. The resultant Co/NBC-900s have Tafel slope of 146 mV dec⁻¹ HER. However, the short stability of these catalysts (10 h) is the primary reason for their restricted applicability[113].

The performance of MOF composites made by graphene oxide (GO) and carbon nanotubes (CNTs) has been the subject of much investigation, although the results have been inconsistent. The catalytic activity of MOF channels can be improved by placing nanoparticles of sulfides, phosphides, and nitrides in those channels. In this technique of production, MOFs play the role of a scaffold for the nanoparticles, which enables the final dimensions of the nanoparticles to be carefully regulated. The increased immobilization, protection, and selectivity provided by MOFs contribute to the increased stability of NPs. By increasing the conductivity of the MOF, these loaded nanoparticles make HER electrocatalysis more efficient. Pd nanoclusters were immobilized on MOF-67 by Zheng et al., which resulted in the production of a composite material (Pd@MOF-74) with increased electrocatalytic activity[114]. Tannic acid shells can be modified by adding metal cations such as nickel, cobalt, copper, manganese, iron, and/or tin. This would result in different chemical compositions. Thermolysis led to the creation of multi-component metal nanoparticles in the metallic fraction of tannic acid, and nanoparticles of platinum served as a seed for this formation. Thermolysis of the organic precursor components was required to create the nitrogen-doped porous carbon capsules with hollow interiors that were determined to constitute the support structure for the nanoparticles. The final catalyst exhibited significantly increased electrocatalytic activity concerning HER[115]. Additionally, MoS_x was solvothermal grafted onto Zr-based MOFs, which led to an improvement in the performance of the HER (125 mV onset potential at 10 mA cm⁻² cathode current and 59 mV dec⁻¹ Tafel slope at 200 mV overpotential) [116]. This was discovered while the researchers were studying the performance of HER.

Table 1: MOF-based catalysts performance Summary

Sr. No.	Catalyst Hybrid	Medium and Study Type	Overpotential (10 mA cm ⁻²)	References
1	Ni-Fe-Mn-MIL-53	KOH (1M) OER study	236	[117]
2	Fe-Ni-MOFs	KOH (1M) OER study	221	[118]
3	Cu-MOF with Fe(OH) _x	KOH (1M) HER	112	[119]
4	MOF/Pt	KOH (1M) HER	28	[120]
5	BDC/Co	OER	241	[121]
6	BDC-Ru-Ni	HER	36	[122]
7	MOF-74/Fe-Co	OER	280	[123]
8	Ni-MOF/Co	OER	240	[124]
9	Ni-MOF/Br	OER	306	[125]

2.3. Cu-Based Catalysts for Water Splitting

In contrast to the OER, which makes use of Cu-OH and Cu-O, HER research is restricted because the copper surface has low ionic conductivity. Graphene and other conducting substrates, innovative methods of synthesis, and the incorporation of other transition metal oxides are some of the potential solutions that have been investigated to lower HER overpotentials and overcome this resistance in Cu-based oxides. When looking at the electrocatalytic activity of HER in alkaline environments, the following pattern was discovered: The following polymers are ranked from excellent to worst: P-Cu (metal) is superior to E-Cu (poly) and A-Cu (poly) (poly). In the XPS investigation, readings that were indicative of the Cu(I) oxidation state (917 eV for the Auger Cu LMM) and the Cu₂O oxidation state (919 eV) were discovered. Researchers were able to characterize the surface chemistry of these electrodes so that they could be used in HER research by

analyzing the relative intensities that were measured. At high concentrations, Cu(0) is more dominant than Cu(I), whilst Cu(I) is less dominant, in all three types of A-Cu (poly), E-Cu (poly), and P-Cu (poly) catalysts. Cu(I) is less dominant at lower concentrations. This suggests that the increased HER activity in P-Cu (poly) was ensured by the presence of excess Cu(I). The O1s XPS high-resolution spectra were used to study hydrophilic characteristics, and the results showed that the surface became more hydrophilic after polishing with P-Cu (poly), in comparison to the less active E-Cu (poly) (poly). This study adds to the expanding amount of data that rough Cu-based catalysts can increase HER's hydrophilic properties by pulling in additional electroactive molecules. The body of evidence is growing because of this discovery.

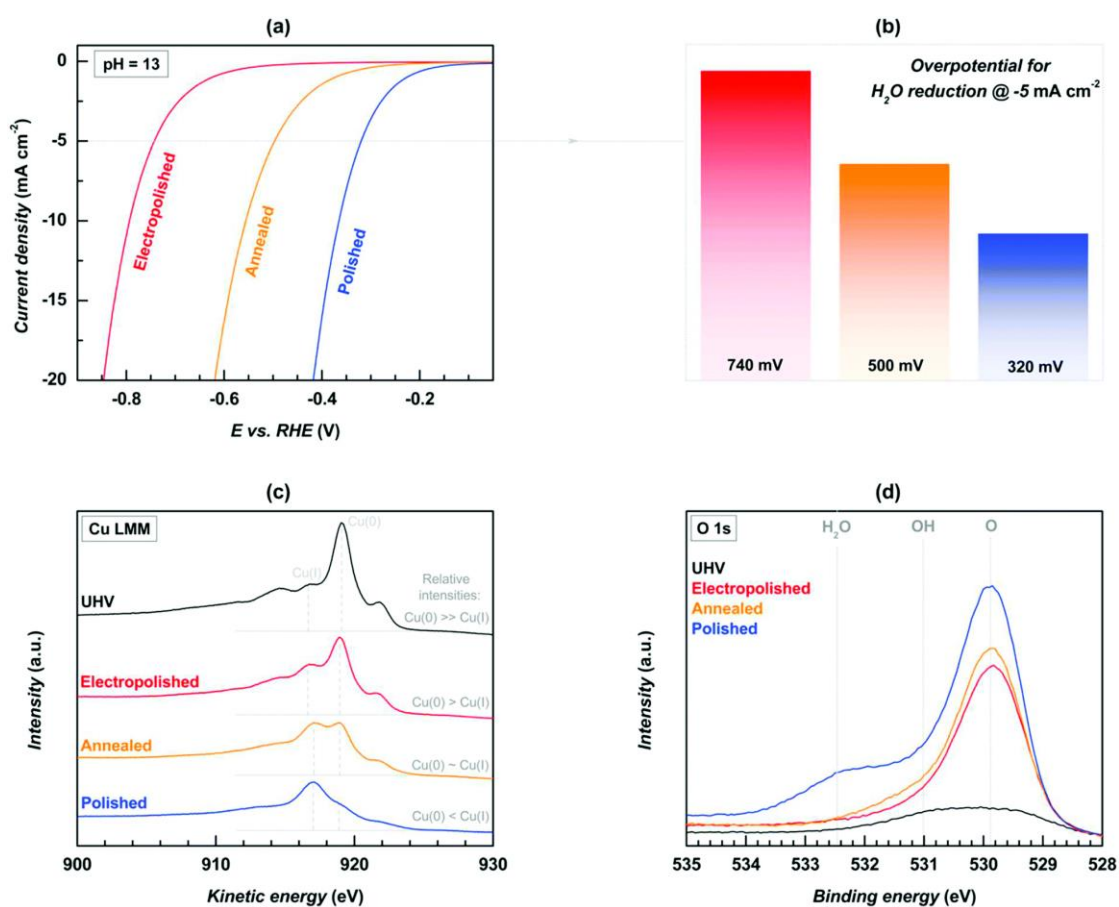


Figure 4 Analysis of Cu-LMM [126]

Copper oxides were coupled with reduced graphene oxide, a metal-organic framework (MOF) porous network, and three-dimensional copper foam by Ye et al. to boost the HER activities of the copper oxides. This work is quite intriguing[127]. After developing a

MOF network on top of the Cu foam, the next step was to add GO in between the two layers to complete the sandwich, which consisted of Cu, Cu, MOF, and GO. It was discovered that Cu/Cu₂O-CuO/rGO, which was created after additional annealing, is an effective HER catalyst when subjected to basic conditions. In a similar vein, Figure 5b suggests that conducting supports such as rGO might improve the kinetics of HER. Further evidence of the superiority of the Cu/Cu₂O-CuO/rGO catalyst in HER can be seen in the fact that it has the lowest R_{ct} among all the catalysts that were tested (Fig. 5c). The catalyst's reliability was validated by a rock-solid consistency, which was observed during a chronoamperometry test that lasted for 14 hours (Fig. 5d). This was in part due to the 3D rGO network's outstanding electrical conductivity, which ensured rapid charge transfer alongside robust activity and structural integrity. This was one of the reasons why this was the case. The findings of this study clear the path for the development of copper-based oxides on metal-organic frameworks (MOFs) and other conductive substrates. This will allow for increased HER activity and stability in basic conditions.

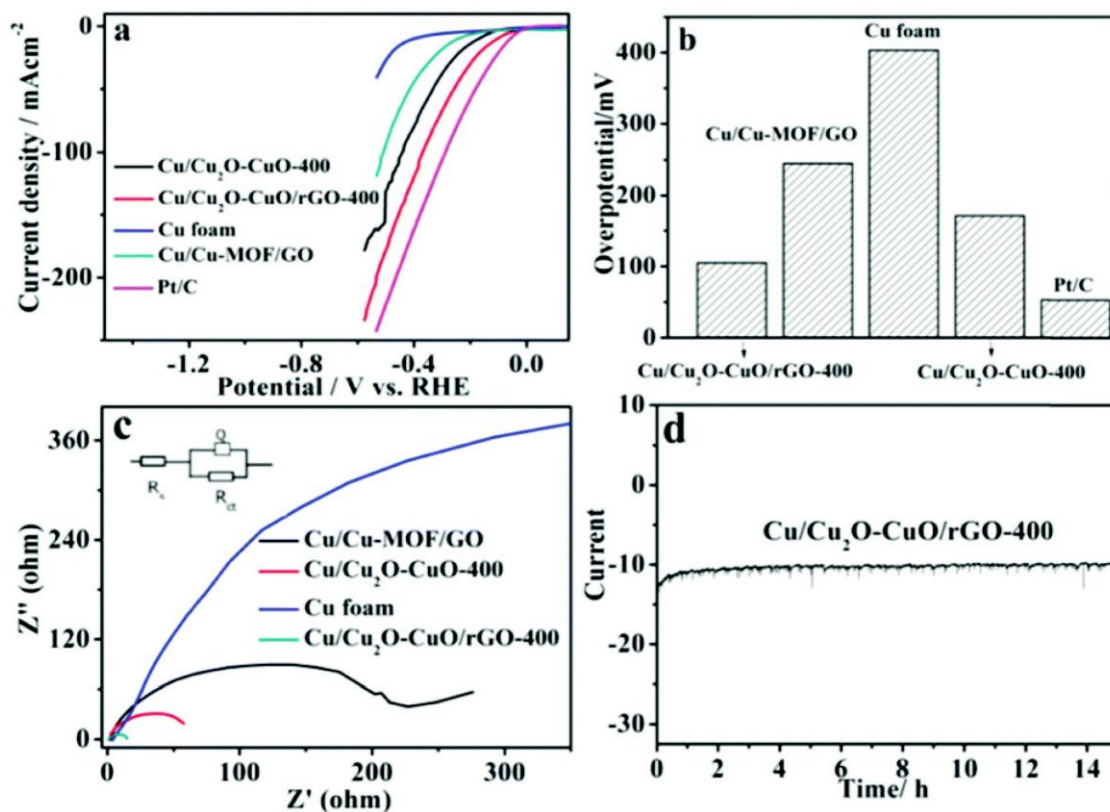


Figure 5 Analysis of Cu-LSM for HER, OER, and Stability [127]

Nanocomposites have the potential to increase HER activity when applied to alkaline media. Tahira et al. [128] utilized the dip-coating process to synthesize $\text{Co}_3\text{O}_4\text{-CuO}$ nanocomposites, which demonstrated promising activity in HER. Low HER activity was demonstrated by both Co_3O_4 and CuO ; however, the $\text{Co}_3\text{O}_4\text{-CuO}$ nanocomposites required only 288 mV to reach 10 mA cm^{-2} in current density (Fig. 6a). They concluded that the increased activity was brought on by the synergistic boost brought about by the combination of cobalt and copper. The Tafel slope measurements show that the charge transfer kinetics of $\text{Co}_3\text{O}_4\text{-CuO}$ nanocomposites (65 mV dec^{-1}) follow a pattern that is comparable to those of $\text{Co}_3\text{O}_4\text{-CuO}$ and CuO (Fig. 6b). In addition, the composites showed enhanced stability throughout both the potentiodynamic and the galvanostatic trials. These copper oxides for HER research have shown promise for the creation of future catalysts by drawing attention to the necessity of certain modifications that would lead to a greatly higher level of HER activity. Incorporating conducting supports, embedding in three-dimensional foam, utilizing nanocomposites, and other alternative approaches are all being studied as potential ways to improve the performance of Cu-based oxides in HER.

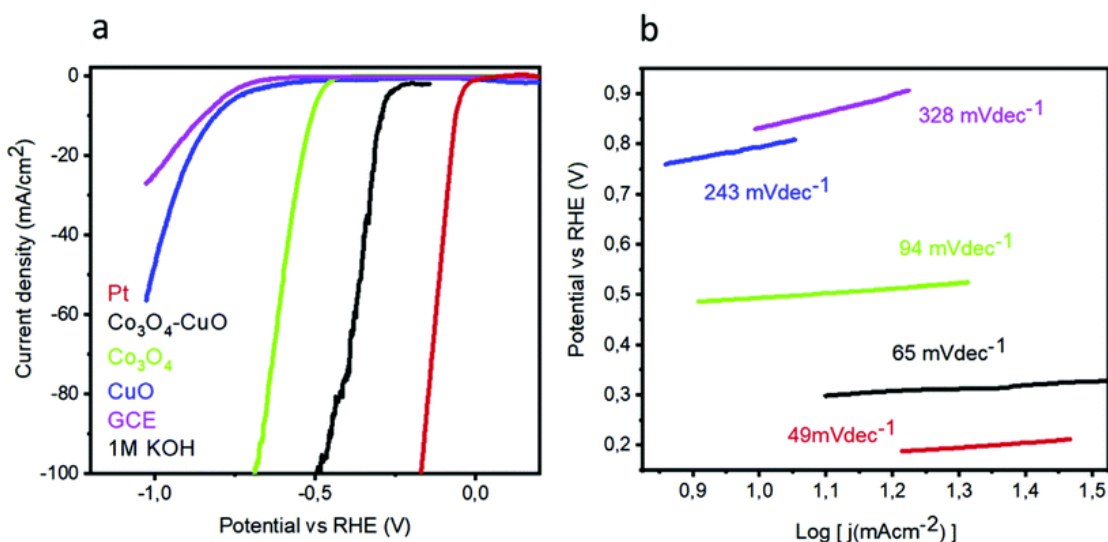


Figure 6 (a) LSV and (b) Co_3O_4 , CuO , and $\text{Co}_3\text{O}_4\text{-CuO}$ nano-based composites Tafel slopes (reproduced with permission from Elsevier, copyright 2019) [128]

2.3.1. Cu-Based layered double hydroxides for OER and HER

The layered double hydroxide catalyst makes it possible for OER and HER to occur by providing a pathway and space for the electrolyte ions to come and intercalate. This is

made possible thanks to the fact that the layered double hydroxide catalyst The hydrophilic qualities can be amplified by including a higher proportion of water, and the interlayer distance can be modified by adjusting the proportions of cations to anions present in the compound. The production of Cu@CoFe LDH for TWS can be accomplished with little effort by employing either an electro reduction or an electrodeposition technique. Annealing the CuO@Cu foam that was produced after Cu(OH)₂ was grown on Cu foam was necessary to bring forth the material's full potential. The addition of electro-reduction resulted in the creation of copper nanowires embedded in the copper foam. The previously described core-shell nano architectures were produced by the utilization of Co and Fe metal precursors during a subsequent cycle of electrodeposition. The effects of these catalysts on OER, HER, and TWS were investigated while they were in an aqueous solution containing 1 M KOH. OER polarization tests discovered that the activity of Cu@CoFe LDH was much higher when compared to that of Cu foam, Cu NWs at Cu foam, and CoFe LDH at Cu foam. This was the conclusion reached after comparing the three systems. The electrodeposited Cu@CoFe LDH samples that were put to the test showed that the 60-s sample had the maximum activity. The accuracy was verified by a chronopotentiometry study that lasted for 24 hours and found that there were no discernible changes in potential during the experiment. An investigation using chronoamperometry that lasted for 30 hours demonstrated the HER's. The HER's activity almost did not decrease at all throughout the experiment, which indicates that the activity was very stable. An electrolyzer that used a Cu@CoFe LDH-60 as both the anode and cathode needed only 1.681 V to function, which is 60 mV higher than an electrolyzer that used an IrO₂ anode and a Pt cathode when the current density was 10 mA cm⁻² (Fig. 7a). In this study, researcher perform a chronopotentiometry analysis on both systems at a current density of 10 mA cm⁻² to investigate the stability requirements for Cu-based catalysts in a two-electrode set-up extreme. Stability was maintained with minimal degradation for up to 48 hours when Cu@CoFe LDH-60 was used as both the anode and cathode in the system; however, the overpotential in the IrO₂/Pt system rapidly increased after 12 hours of operation. Cu-based LDHs certainly show promise given that their predicted faradaic efficiencies are so close to reaching 100%. In addition to having a larger Cdl and a lower R_{ct}, it was found through a computation that the Cdl in EIS is more

promising for prospective future uses. This finding comes after the discovery that the R_{ct} in EIS is lower (Fig. 7b–f). The significance of utilizing Cu-efficient TWS in an alkaline setting was demonstrated by this line of research, which validated its importance. Another observation made by the same group[129] concerned the use of Cu@NiFe LDH for TWS generation in 1 M KOH. In this illustration, the LDH structure was produced by depositing a highly active metal precursor, NiFe, on top of a Cu foam. The Cu foam served as the substrate for the LDH structure. To briefly recap, the Cu@NiFeLDH/Cu foam was manufactured using a process that included electro-reduction as well as electrodeposition. The required overpotential for OER was 199 mV when the current density was 10 mA cm^{-2} , yet the Tafel slope value was only 27 mV dec^{-1} , indicating that approximately four electrons were transported at this current density. The overpotential for HER was measured to be 116 mV when 10 mA cm^{-2} was applied, and the Tafel slope was 58.9 mV dec^{-1} . Both OER and HER exhibited a high degree of consistency with one another. The findings of the TWS showed that the Cu@NiFe LDH system only required 1.54 V between the anode and the cathode to attain 10 mA cm^{-2} current density, in contrast to the IrO_2/Pt system, which required 1.63 V between the anode and the cathode. The dependability of the Cu@NiFe LDH electrodes has been established using post-structural testing such as mapping, HRTEM, and XPS (Fig. 7a–e). The mapping research unearthed every feature that had been predicted to be there. During the process of reevaluating the stability of the polarization curves, evidence of OER and HER activity was found. A comparison of the OER and HER LSV curves reveals that the shifts that were found to have occurred were not particularly large (Fig. 7f). The results of these experiments, which compare LDH structures based on copper to those based on other transition metals, are positive since they open the way for the potential straightforward commercialization of these structures in the not-too-distant future.

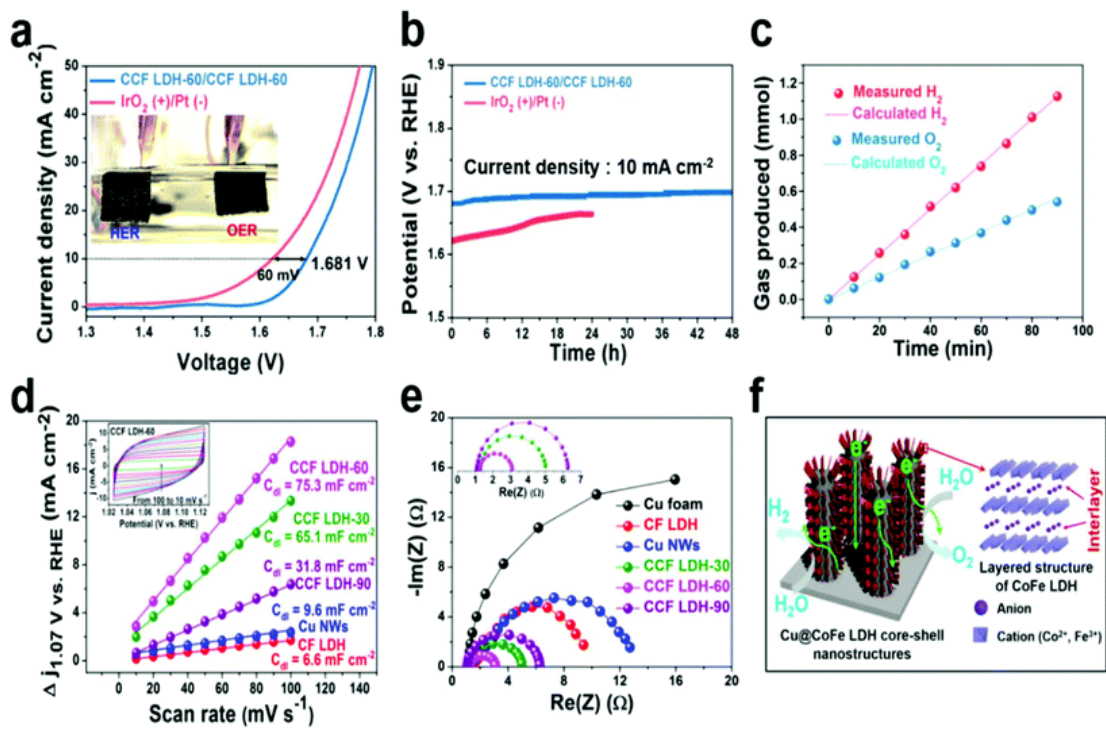


Figure 7 (LSV, efficiency, Resistance plot, GSTAT, and structure) [130]

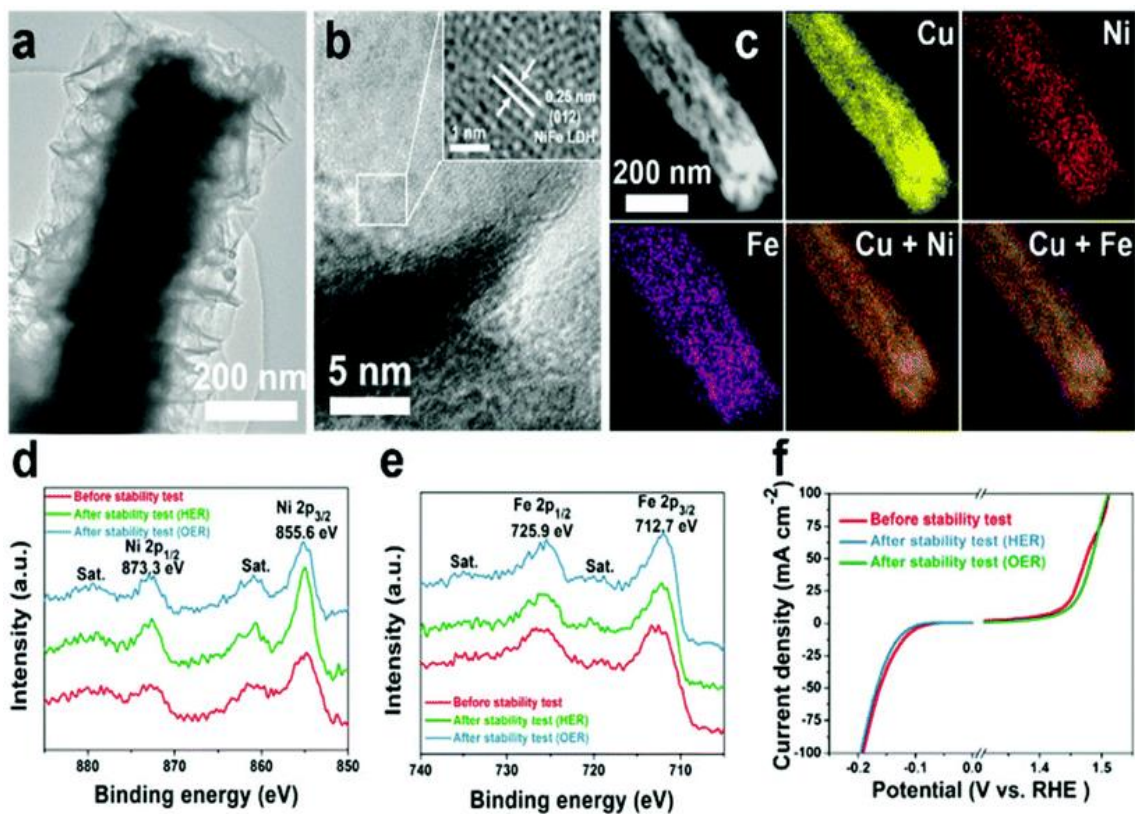


Figure 8 (Analysis of the Cu-Co-Fd-DH) [129]

Additionally, it was discovered that the OER activity of NiFe LDH that contained copper in the form of $\text{Cu}(\text{OH})_2$ was boosted when it was mixed with potassium hydroxide. $\text{Cu}(\text{OH})_2@$ NiFe LDH was grown by Ma et al. [20] on carbon paper by employing a modification of the unipolar pulse electrodeposition (UPED) technique. Adjustments were made to both the power consumption during deposition and the Ni/Fe feeding ratio. The OER activities of $\text{Cu}(\text{OH})_2$ that had been deposited on NiFe LDH/CF were also investigated. Depositing $\text{Cu}(\text{OH})_2@$ NiFe LDH over carbon paper was accomplished using several techniques, including atomic layer precipitation evaporation deposition (UPED), the potentiostatic method (PM), cyclic voltammetry (CV), and the pulse potentiostatic method (PPPM) (PPM). The OER activity of each of these catalysts, which were produced by varying the stoichiometry and the amount of energy applied, has been investigated. During the deposition process, the OER activity connected to the consumption of 2.5 °C of energy was found to be greater than that seen for any other amount of power that was used. In addition, when the CV technique, the PM method, and the PPM method were

compared to the UPED method, it was found that the UPED method was the most effective for depositing $\text{Cu}(\text{OH})_2@ \text{NiFe}$ LDH. This was determined while comparing the UPED method to the CV method, the PM method, and the PPM method. The UPED method of testing revealed that a ratio of 6:4 Ni/Fe is optimal, with an overpotential of approximately 283 mV at a current density of 10 mA cm^{-2} and a Tafel slope value of 88 mV dec^{-1} that is lower than that of all other materials,

except for $\text{Cu}(\text{OH})_2$ and NiFe LDH. These values were determined using a current density of 10 mA cm^{-2} . The benefits of combining NiFe LDH and $\text{Cu}(\text{OH})_2$ were proved by the findings of a continuous electrolysis stability test that lasted for ten hours. After long-term, continuous electrolysis, only $\text{Cu}(\text{OH})_2$ was degraded in the $\text{Cu}(\text{OH})_2@ \text{NiFe}$ LDH reaction because NiFe LDH prevented $\text{Cu}(\text{OH})_2$ from leaching. The OER and HER activities can be improved by mixing superstructures based on Cu with those based on Ni, Fe, and Co, all of which are transition metal LDHs. Copper, when combined with highly active Ni to produce NiCu LDH, has been the subject of intense research for its potential applications in OER. Following the production of NiCu LDH, the brucite layer was cleaned of Cu(II) by employing a straightforward ion-reductive complexation extraction (IRCE) technique [131].

Ni- Cu_x LDH was developed as a solution to fill this void in the industry's requirements, and it catalyzed OER to produce exceptionally high levels of OER activity. NiCu LDH exhibits low levels of OER activity, just like $\text{Ni}(\text{OH})_2$ does. Although the exfoliation process reduces the mechanical stability of LDH structures and, as a result, their OER activity, it has the potential to increase the activity of less active LDHs, such as NiCu LDH, by introducing flaws into the material. In this instance, the complexation of an ionic extractant led to the formation of vacancies rather than a change in the structure itself. The disruption of the transition metal-based LDH structures is avoided because of this, which is a useful effect. An overpotential of approximately 343 mV is required to obtain 10 mA cm^{-2} for OER when using only NiCu LDH. The development of vacancies in SAV-Ni- Cu_x LDH led to a reduction in the overpotential to 290 mV when the current density was 10 mA cm^{-2} . The Tafel slope for the NiCu LDH was 83 mV dec^{-1} , while for the SAV-Ni- Cu_x LDH, it was a much more manageable 45 mV dec^{-1} . Simply applying an overpotential of 355 mV was sufficient for the SAV-Ni- Cu_x LDH to achieve a current density of 100

mA cm². Since we now know how to produce LDHs utilizing catalysts based on copper, we may employ vacancy engineering to significantly boost their activities for oxygen evolution reaction (OER) without changing the surface of the LDHs. In response to this challenge, researchers have developed unique techniques for creating highly active NiCu LDH nanostructures. One example of this is the modification of the synthesis technique. Zheng et al. [132] utilized a solvothermal growth method to successfully cultivate NiCu LDH directly on carbon fabric. A Tafel slope of 42.5 mA cm⁻² was achieved by using an overpotential of only 290 mV when the current density was 10 mA cm⁻². The results of the stability test offer further evidence that NiCu LDH for OER can be relied upon as a reliable reagent. According to the findings of the researchers, the OER activity of trimetallic LDH is significantly higher than that of bimetallic LDH.

Hu et al. [133] developed procedure which is carried out on nickel foam. This study focuses on hybrid electrolysis ways to lessen the environmental impact of OER alone. Some examples of hybrid electrolysis approaches include ammonia electrolysis, urea electrolysis, and hydrazine electrolysis. Overpotentials of 460 mV were required for 100 mA cm⁻² in OER when utilizing N-NiZnCu LDH/rGO, but in HER, the same current density required overpotentials of 196 mV. Ni-Zn-Cu lyase/uridine dehydrogenase/glutamate (N-NiZnCu LDH/rGO) When we did a comparison using a configuration with two electrodes, we discovered that the voltage needed to reach 100 mA cm⁻² was 1.974 V. These findings demonstrated that trimetallic LDH systems, which utilized copper (Cu) as the transition metal, were successful in enhancing both OER and HER. Additionally, it was discovered that cationic vacancies could be created on the surfaces of LDHs using different methods without disrupting the LDHs' surface by using different methods. In addition, the stability of copper-based LDHs was demonstrated to be more obvious than the stability of copper-based oxides and hydroxides. There is still the possibility of boosting LDH activity by modifying the copper-based surfaces of the organisms.

2.3.2. Cu-Based phosphides for OER and HER

Because of its high electrical conductivity and metalloid composition, the metalloid copper phosphide has been the focus of substantial research for electrocatalytic water splitting. A synergistic increase of the OER is observed while utilizing transition metal

catalysts based on phosphide compounds. In addition, the phosphide (P_3) ions that make up HER can swiftly and efficiently bind protons. Tian et al.[134] demonstrated that copper foam may be used well as an electrode for HER in acidic environments. These researchers demonstrated that it is possible to generate arrays of Cu_3P nanowires directly on top of the foam. Since Cu and the pendant base P were so effective at catalyzing the reaction, it was determined that they are to blame for the increased HER activity. The benchmark for this experiment was microparticles composed of the substance Cu_3P . Cu_3P NA/CF had an attenuation threshold of 62 mV when subjected to a current density of 10 mA cm^{-2} , whereas Cu_3P MP/CF had a threshold of 190 mV. Cu_3P NA/CF required just 67 mV dec^{-1} to enhance electron transport, but Cu_3P MP/CF required 96 mV dec^{-1} to accomplish the same goal. These findings demonstrate that HER nanostructures that include many active sites and can be accessed electrochemically are extremely useful. According to the findings of the rate stability investigation, the Cu_3P -based catalysts were extremely stable, with the LSV curve indicating nearly little activity loss after multiple cycles. It is possible to boost the HER activity of these phosphides based on copper by adding in other phosphides based on transition metals. According to the results of an intriguing study conducted by Chu et al.[135], $Ni_{2x}Cu_x$ -P nanosheets were utilized to increase HER activity in an alkaline medium.

The development of NiCu LDH on top of Ni foam was part of the work that was done here, and the resulting $Ni_{2x}Cu_x$ -P/NF was used in HER applications once it was phosphorated as shown in figure 15. The HER of the NiCu LDH has improved thanks to an overpotential that was 136 mV. Overpotentials of 103 mV were necessary for Ni₂P, whereas 117 mV were necessary for Cu_3P . Phosphorization, as was the case before, demonstrates an improvement in activity compared to NiCu LDH. To produce $Ni_{2x}Cu_x$ -P/NF, we altered the atomic ratio of Ni to Cu. Ni_{1.8}Cu_{0.8}P/NF had the highest level of activity among them, needing only 78 mV of overpotential to generate 10 mA cm^{-2} of current. In addition, in comparison to NiCu LDH and mono-metallic phosphides, the observed Tafel slope is a significant amount flatter at 70 mV dec^{-1} . Despite being subjected to a cycle study, the bimetallic phosphides did not appear to have undergone any major changes. In this scenario, Cu modifies the Fermi level to facilitate H_2 desorption.

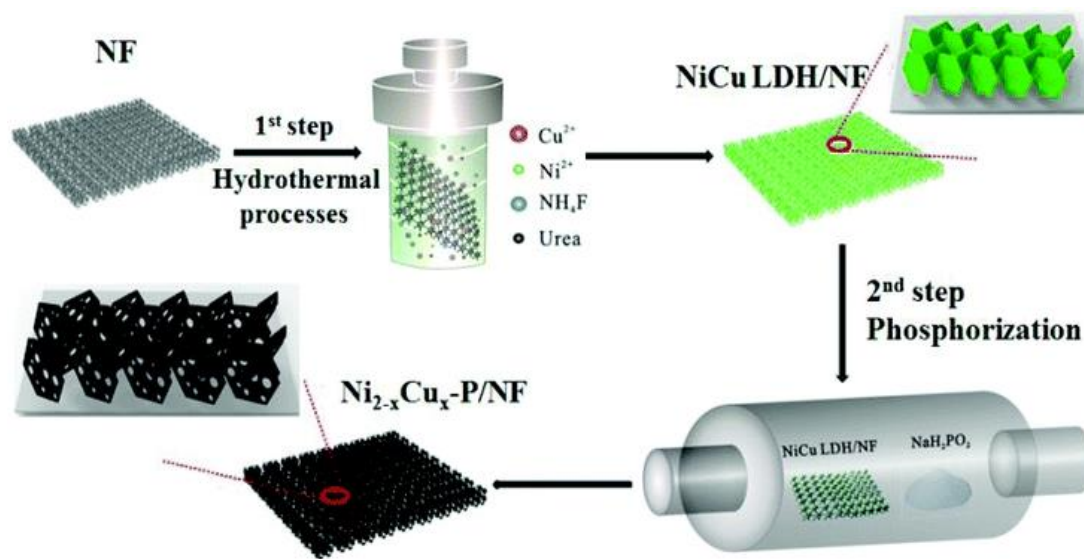


Figure 9 Preparation of NiCu phosphide over NF for HER reaction (reproduced with permission from ACS publications, copyright 2017) [136]

These findings imply that the activity of HER might be further improved by modifying the stoichiometry and that Ni_{2x}Cu_x-P/NF could benefit from the addition of a variety of transition metals as catalysts for HER. It will be interesting to see if the TWS can be applied to Cu-based phosphides has focused on other transition metal-based phosphides, such as Ni and Co, so it will be interesting to see if the TWS can be applied to Cu-based phosphides. Hydrothermal treatment, followed by high-temperature phosphorus conversion, was the method that Han et al.[136] used to synthesize Cu₃P/NF. The slope of the Tafel chart was around 42 mV dec⁻¹, and the required overpotential for HER was 105 mV. Because of Cu₃P/high NF's OER and HER activity, TWS has chosen to use it as both the anode and the cathode in their TWS reactor. It was possible to achieve a current density of 10 mA cm⁻² at an overvoltage of 1.67 V, which is equivalent to an overpotential of only 440 mV. In addition, the initial overpotential for TWS using Cu₃P/NF electrodes was only 270 mV, which is a relatively low value (Figure 16 a–d). After 10 hours of bulk electrolysis, Cu₃P/reliability NFs in industrial water splitting were also validated. As a direct consequence of these findings, Cu₃P has been investigated for its potential application as a stand-in for several transition metal-based catalysts, such as Ni and Co. When searching for precious metals to replace, copper phosphides provide the impression of being a promising alternative to other potential replacements. They are also resistant to breakdown in settings that are both acidic and alkaline, which adds to the possibility that

they could be used as alternatives. It's possible that in the future, TWS with copper-based catalysts will be the way to go for making the most of limited resources. These phosphides based on copper can be utilized either on their own or in conjunction with other catalysts based on transition metals.

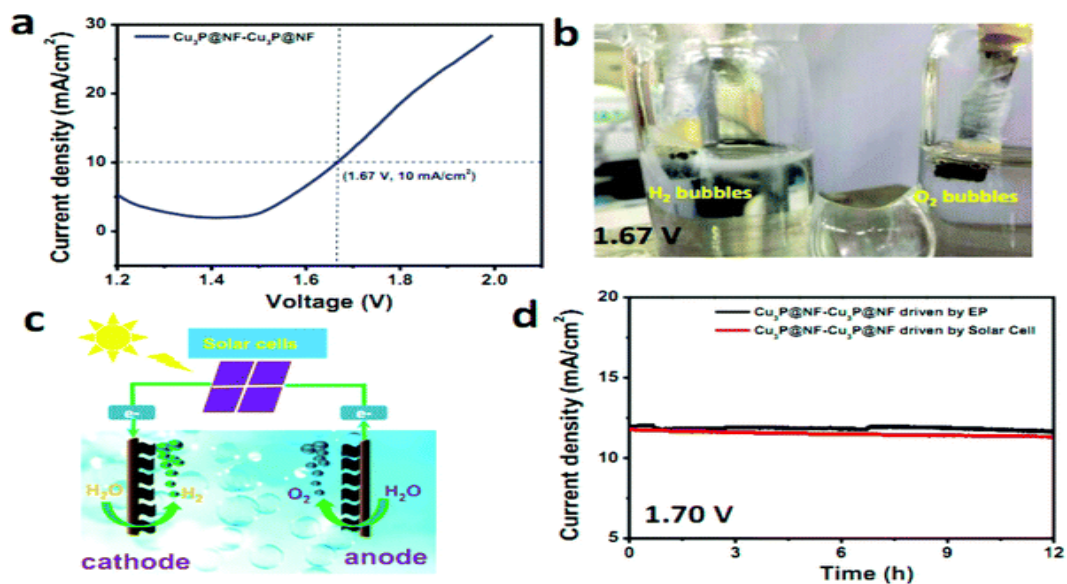


Figure 10 (a-d) LSV, Cu₃P catalysts in KOH for two-electrodes, the scheme, and PSTAT analysis for 12 h (reproduced with permission) [136]

Cu-based tellurides have not been investigated as thoroughly as sulfides and selenides. The formation of Cu_{2x}Te catalysts for HER in acidic electrolytes has been emphasized by Kumaravel et al. [137]. Cu_{2x}Te catalysts were produced using wet-chemical and hydrothermal methods, and their activities were compared. Hydrothermal production of Cu_{2x}Te from Cu metal precursors in the presence of NaBH₄ and Te salts was achieved for the first time at room temperature. The homogeneous distribution of Cu and Te is supported by the observed HAADF mapping model. However, oxide generation cannot be prevented, which may dampen the potential of HER study. The effectiveness and longevity of telluride-based Cu were then investigated by HER. Compared to Cu_{2x}Te/WC, which required 432 mV to get the same current density, the generated Cu_{2x}Te/hybrid demonstrated significant activity by achieving an overpotential of 347 mV. (HER performance is amazing). The larger prevalence of the facile charge transfer phenomenon in Cu_{2x}Te/hybrid is also indicated by the larger value of the Tafel slope, which is 188 mV

dec⁻¹. Computational studies of electron impact spectroscopy (EIS) and electron correlation spectroscopy (ECS) revealed that the larger exposed active surface area of Cu₂xTe/substantially hybrid promoted faster electron transfer kinetics. In addition, potentiostatic analysis was utilized to measure the stability, and it was determined to be rather high for 12 hours with no variation in activity. This study employed a variety of synthetic methods to show that tellurides based on copper are necessary for evaporation control. As we have shown in our studies of Cu-based selenides, the activities of these Cu-based tellurides can be further enhanced by increasing the metallic sites, expanding over 3D structures, using conducting supports, and extending with other transition metal-based tellurides. For both OER and HER, it is highly desirable to develop Cu -based tellurides as a means of lowering energy inputs. Majhi et al.[138] investigated the HER of hydrothermally produced CoTe₂@CuTe and FeTe₂@CuTe nanocomposites in acidic, alkaline, and neutral electrolytes. The CoTe₂@CuTe catalyst required only 58.1 mV of overpotential for the HER studies conducted under acidic conditions, while the FeTe₂@CuTe catalyst required 86 mV. When compared to selenides (CoSe₂@ CuSe₂ and FeSe₂@ CuSe₂), the overpotential was still quite high at 117 and 127.7 mV. As a result, tellurides based on copper and other transition metals had a more significant effect on HER than their selenide counterparts. In a similar vein, the overpotential required by CoTe₂@CuTe was 125 mV, whereas it was 203 mV for FeTe₂@CuTe at the same current density in neutral circumstances. Again, selenide analogs required far greater overpotentials compared to their telluride counterparts (225 and 252 mV, respectively). CoTe₂@CuTe and FeTe₂@CuTe required overpotentials of 106 mV and 122 mV at 10 mA cm⁻², respectively, in alkaline conditions; equivalent selenides required overpotentials of 129 mV and 180 mV, respectively.

2.3.3 Ru-modified Cu-BTC

A carbon skeleton was created by pyrolyzing a Ru-modified Cu-BTC precursor in N₂. This carbon skeleton enclosed bigger Cu nanoparticles as well as ultrasmall Ru nanoparticles (henceforth termed S-0). Some of the Ru nanoparticles were converted into RuO₂ through a process called annealing, which was carried out in the air. It was confirmed that the CuO nanoparticles lacked catalytic activity for HER and OER by etching them with three times the concentration of hydrochloric acid. In the end, the

researcher was able to procure the Ru/Cu-doped RuO₂ catalyst that was needed to perform the water-splitting reaction. The overall performance of the water-splitting electrocatalyst is superior to that of state-of-the-art electrocatalysts. To attain current densities of 10 and 100 mA cm⁻², respectively, only 1.47 and 1.67 V are required. According to the findings of the DFT study, doping RuO₂ with Cu has the potential to increase its OER performance. This is because it enables fine-tuning of the d-band center, which, in turn, modifies the electronic structure of the Ru activity sites on the RuO₂ (110) plane[139].

2.3.4. Channel-rich RuCu nanosheets

Researchers were able to construct channel-rich RuCu nanosheets by using a wet chemical approach. These nanosheets are formed of crystalline Ru and amorphous Cu, and they feature many channels that may be accessed (denoted as RuCu NSs). The electrochemical performance of the optimized RuCu NSs is significantly higher when contrasted with that of their OER and HER counterparts. The RuCu NSs/C that were optimized at 350 °C showed activity that is desired for OER, while the RuCu NSs/C that were optimized at 250 °C showed activity that is desirable for HER. In water splitting applications utilizing the enhanced RuCu NSs/C, 10 mA cm² is reached at 1.48 V, 1.55 V, 1.49 V, and 1.50 V, respectively, in 1 M, 0.1 M KOH, 0.5 M, and 0.05 M H₂SO₄, when compared to those applications utilizing the RuCu NPs/C and commercial Ir/C||Pt/C. These voltages are attained in 1 M, 0.1 M, and 0.05 M KOH, and after being subjected to long-term dependability tests, the optimized electrolyzer has been shown to maintain a steady overpotential with very little variation because of the tests' findings[140].

2.3.5 Ru-doped Cu electrocatalysts

To make a Ru-Cu@C-1 sample, a RuCu-BTC-1 precursor was annealed at 500 °C for three hours in nitrogen at a heating rate of two degrees per minute. RuCu-BTC-2 and RuCu-BTC-3 precursors, which are very similar to Ru-Cu@C-1 precursors, were utilized in the production of RuCu-BTC-2 and RuCu-BTC-3 samples, respectively. The optimized Ru-Cu@C-2 catalyst has been proved to be an excellent HER catalyst because of its ultralow overpotential (20 mV at 10 mA cm⁻²), ultralow Tafel slope (37 mV dec⁻¹), minor charge-transfer resistance (16.8), broad electrochemical active surface area, and superb stability. All these characteristics contribute to the catalyst's exceptional performance[141].

2.3.6 AB & Cu-MOF composite

In a solution that included 2.5 mL of dimethylformamide, 2.5 mL of water, and 2.5 mL of ethanol, 20 mg of $\text{Cu}(\text{OAc})_2$ and 21 mg of 1,3,5-benzene tricarboxylic acid were dissolved. Different results were obtained by altering the proportion of AB that was added to the mixtures (0.4, 0.7, and 1.7 wt.%, respectively, based on Cu-BTC). After being sonicated, the substance was put into an autoclave made of stainless steel and lined with Teflon. It was then heated to 100 °C for twenty-four hours. The bluish-gray crystals that were collected were filtered, cleaned, dried, and weighed after being processed in a vacuum oven. The overpotential of the 1.7% AB/Cu-BTC composite is 208 mV when measured at a current density of 10 mA cm⁻², and the Tafel slope is 80 mVdec⁻¹[142].

Chapter 3

Materials and Methods

3.1 Chemicals and reagents

All the chemicals used to synthesis MoP hybrids with RGO were analytical grades. These involved Sodium Molybdate Dihydrate ($\text{Na}_2\text{MoO}_4 \cdot 2\text{H}_2\text{O}$), Sodium Hypophosphite Monohydrate ($\text{NaH}_2\text{PO}_2 \cdot \text{H}_2\text{O}$), Sulfuric Acid (H_2SO_4), Potassium Permanganate (KMnO_4), Graphite powder, Sodium Nitrate (NaNO_3), Hydrogen Peroxide (H_2O_2), and Deionized water.

3.2 Preparation of Pure Cu-BTC

Cu-BTC was synthesized using solvothermal conditions with some modifications in the method used in the literature. For the synthesis of Cu-BTC, 5.2 g of Copper (II) nitrate hemi (III) hydrate and 2.52 g of benzene 1,3,5 tricarboxylic acid was used. These compounds were dissolved in a 125 ml (41.7 mmol of each) solvent mixture of N, N DMF, deionized water, and ethanol. These reactants were agitated at room temperature for 10 minutes and then were sonicated in a sonication bath for 30 minutes. Reactants were then placed in an oven at 60 °C for 24 hours. Later, samples were washed through DMF solvent through a centrifuge for 1 hour and the sample was then dried at 60 °C for 12 hours in the oven. Given below figure 1 provides a schematic of the synthesis of Cu-BTC.

3.3 Preparation of Pure g-C₃N₄

At a pace of 0.5 degrees Celsius per minute, a muffle furnace was utilized to raise the temperature of 10 grams of urea powder to 550 degrees Celsius. Over three hours, the temperature was kept at 550 degrees Celsius throughout. The g-C₃N₄ nanosheets that were obtained were then crushed into a powder once they had been allowed to recover to the temperature of the surrounding environment.

3.4 Preparation of Hybrids Cu-BTC/ g-C₃N₄

For the synthesis of hybrids, 5 mg, 10 mg, and 15 mg of g-C₃N₄ samples were prepared. In the preparation of Cu-BTC/g-C₃N₄, reactants of Cu-BTC were taken as the same as mentioned in the Cu-BTC synthesis, and while agitation, 5 mg, 10 mg, and 15 mg of g-

C₃N₄ were added respectively. After agitation, the sonification time was increased to 1 hour and the rest of the procedure was the same as for Cu-BTC synthesis.

3.5 Characterization and Electrochemical Study

X-ray Diffraction (XRD) (STOE-SEIFERTX'PER PRO) was used to investigate the crystallinity of the synthesized materials and conduct a compositional analysis. Cu-K radiation was used for compositional analysis, and the angle 2θ values ranged from 5° to 85°. The surface morphology and structure of the catalysts were observed using Scanning Electron Microscopy (SEM) (JEOL-JSM-6490A) connected with Energy Dispersive X-ray (EDX) analysis. The ink was made to conduct the electrochemical study on the prepared samples. Polyvinylidene fluoride (PVDF) (2.5 mg) and N-methyl-2-pyrrolidone (NMP) (3 mL) were mixed. The mixture was stirred for 1 h after adding an active catalyst (42 mg) and carbon black (5 mg). After 4 h of sonication, the solution was deposited on both sides of the nickel foam and dried overnight at 70°C. An electrochemical study was carried out on a 3-electrode OrigaMaster potentiostat. Pt and Ag/AgCl wire were employed as counter and reference electrodes, respectively, including active catalyst as the working electrode. The catalytic activity of three electrodes in an alkaline solution containing 1 M KOH was examined at various scan rates. The conventional Reversible Hydrogen Electrode (RHE) potential was determined to simplify the calculation using Eqn. (7).

$$E_{\text{RHE}} = E_{\text{Ag/AgCl}} + 0.059 \text{ pH} + 0.1976 \quad (7)$$

The stability of the catalyst was determined using chronopotentiometry studies. EIS was performed using an alternating current (AC) and a Voltage of 10 mV over a frequency range of 200 kHz to 100 MHz. Equation (8) was used to calculate electrochemical surface area (ECSA).

$$\text{ECSA} = C\ddot{o} / C_s \quad (8)$$

$C\ddot{o}$ and C_s show the capacitance of the double layer and per unit area capacitance of a specific flat surface in the range of 0.040 mF/cm².

Chapter 4

Result and Discussion

4.1 X-ray diffraction (XRD)

Fig. 11 depicts the octahedral crystal structure of Meso-Cu-BTC, which was further validated by X-ray diffraction (XRD) experiments. The results showed that the reported XRD patterns in the literature were consistent with the experimental ones, proving that the highly crystalline phase was the product of the solvothermal circumstances[42]. X-ray diffraction research revealed that pure Cu-BTC had diffraction peaks at 6.57° , 9.57° , 11.69° , 13.4° , 14.67° , 17.46° , and 18.96° on the corresponding 200, 220, 311, 331, 400, and 440 reference planes. X-ray diffraction analysis of a 15 mg sample of the g-C₃N₄ in Cu-BTC hybrid revealed crystalline planes at (200), (220), (311), (400), (331), and (440), with corresponding angles of 6.53° , 9.53° , 11.68° , 13.4° , 14.60° , 17.30° , 19.05° , 29.05° . X-ray diffraction analysis on a 10 mg sample of a g-C₃N₄ in Cu-BTC hybrid revealed diffraction peaks at 6.62° , 9.42° , 11.50° , 13.19° , 14.50° , 17.29° , 19.05° , and 29.05° . At 11.68° , the crystallinity peak was found, suggesting a very high purity. There may be a trace amount of Cu₂O phase present, as shown by some faint peaks between 35.4° and 43° , as shown in the inset of Figure 11. Meso-Cu-BTC metal-organic frameworks (MOFs) have been proposed to be produced at elevated temperatures[143], [144]. The crystal size, an important factor in the catalyst's performance, can be calculated from the XRD data. Using Scherrer's equation, the ultimate crystal sizes of the catalyst are determined. The XRD pattern is interpreted with the help of the X-part high score program. Table 2 summarizes the typical sizes of crystals. Since its average crystal size is the smallest of any known catalyst, the catalyst containing 15 mg of Cu-BTC has the highest activity and the largest surface area.

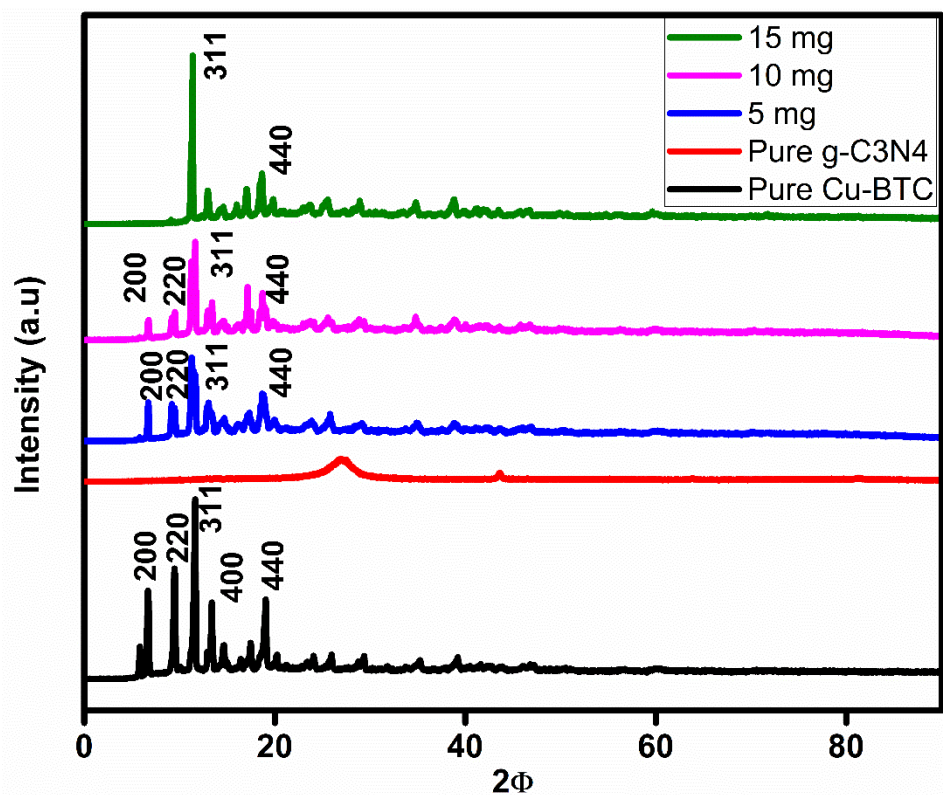


Figure 11 XRD of the prepared samples.

Table 2: Average crystal sizes of the prepared samples.

Electrocatalyst	Peak Position	FWHM	Crystal Size	Average Crystal Size
Pure Cu-BTC	5.845, 6.710, 9.498, 11.645, 19.067	0.146, 0.218, 0.218, 0.146, 0.291.	576, 379, 380, 579, 285.	439.8
Pure g-C ₃ N ₄	24, 43.6	0.14, 0.189	574, 430	502
5 mg Cu-BTC	6.728, 11.260, 18.308, 23.848	0.182, 0.146, 0.109, 0.291	457, 578, 797, 287	529.75
10 mg Cu-BTC	6.728, 11.260, 18.308, 23.848	0.146, 0.218, 0.109, 0.874	577, 380, 797, 94	487

15 mg Cu- BTC	9.137, 11.260, 18.308, 23.848	0.109, 0.731, 0.146, 0.218	789,110, 583, 387	467
--------------------------	-------------------------------------	-------------------------------	----------------------	-----

4.2 Scanning Electron Microscopy (SEM) and Energy Dispersive X-Ray (EDX)

To further study the morphology of our prepared catalysts scanning electron microscopy of the prepared catalysts has been performed. Figure 12 a is the SEM image of pure Cu-BTC and it clearly shows the synthesis of the octahedral shape crystal of the catalyst. This octahedral nature of the catalyst enables a larger surface area of the catalyst and because of that more active site will be available for the hydrogen absorption. Figure 12 (b, c, d) are the SEM images of the prepared hybrids of Cu-BTC with g-C₃N₄ with various weight percentages. 12 b is the hybrid having 5 mg of g-C₃N₄ in Cu-BTC while 12 c and 12d are the SEM images of hybrids having 10 mg and 15 mg of g-C₃N₄ in Cu-BTC respectively. In all the hybrids we can see the perfectly formed octahedral crystal of Cu-BTC along with sheets of g-C₃N₄. To confirm the presence of g-C₃N₄ particles and Cu-BTC both in the hybrids EDX of the hybrid has been performed. Figure 13 a is the EDX of pure Cu-BTC which shows the presence of Cu, C, and O atoms in a weight percentage of 35.8, 38.9, and 25.3 respectively. The atomic percentage of these elements are 10, 60, and 29 % respectively. Figure 3 b is the EDX of a hybrid having 15 mg of Cu-BTC. From this EDX it is confirmed that along with Cu, C, and O an extra element is added, that is N which confirms the synthesis of our hybrid. The weight percentages of all these elements are 34.3, 36.8, 21.3, and 7.6 respectively.

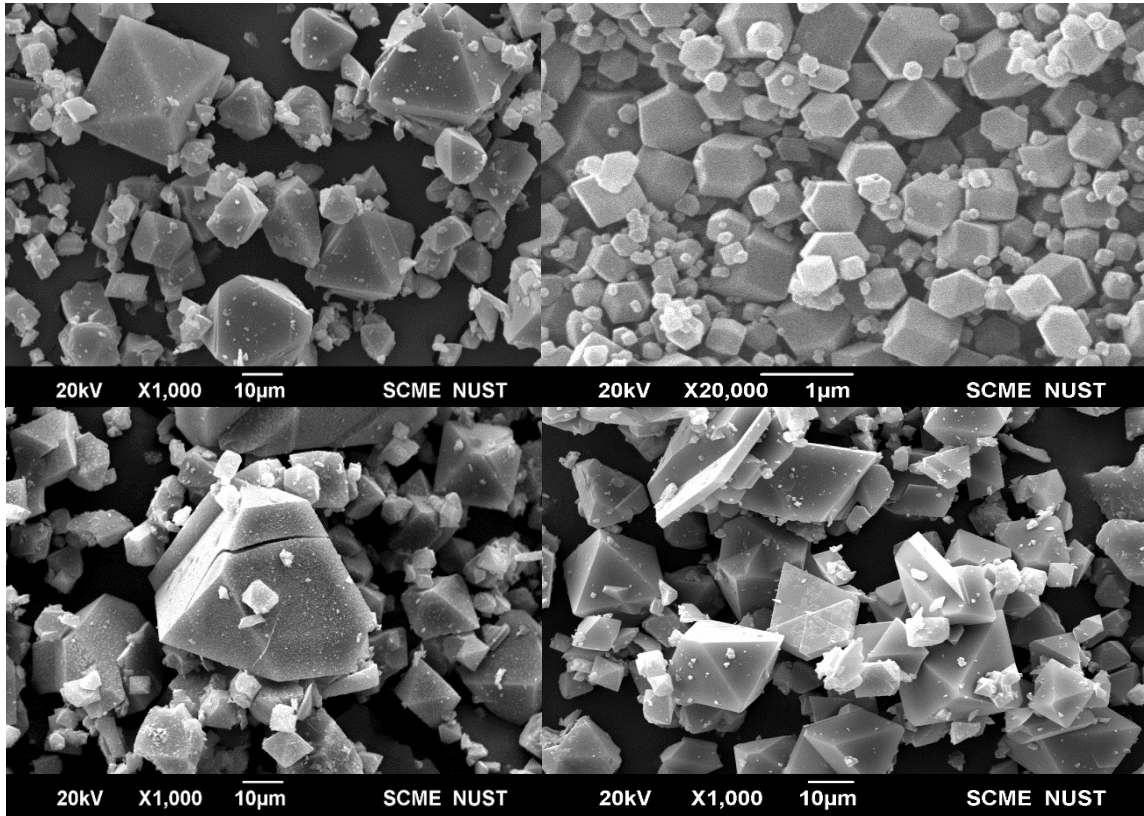


Figure 12: SEM images of Pure Cu-BTC, and hybrid samples

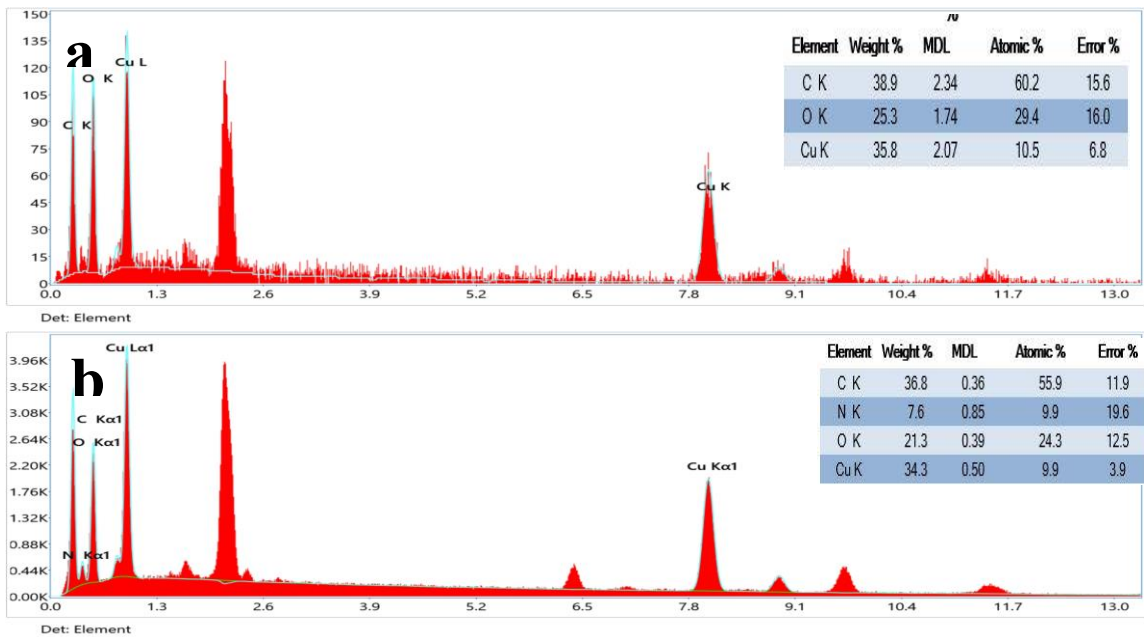


Figure 13: (a) EDS of pure Cu-BTC, (b) EDS of the hybrid having 15 mg of Cu-BTC/g-C₃N₄

4.4 Electrochemical study

4.4.1 Hydrogen Evolution Reaction (HER) and Oxygen Evolution Reaction (OER)

The electrocatalytic activity of the prepared catalysts is found through different parameters in using a 1 molar KOH electrolyte solution. Linear sweep voltammetry (LSV) was performed for both the hydrogen evolution reaction and oxygen evolution reaction for the determination of the overpotential. Over potential is one of the important parameters in the activity of a catalyst. In general, the lower the overpotential of the catalyst the better the activity of that catalyst will be. Figure 14 shows the LSV curve for HER and OER. From Figure 14 (a) it can be seen that the hybrids show better activity as compared to that of the pure Cu-BTC and pure g-C₃N₄ by giving low overpotential at the same current density. The overpotential of pure Cu-BTC and pure g-C₃N₄ are 240 mV and 181 mV at a current density of 10 mA/cm² respectively. At the same current density, the hybrids give overpotentials of 202 mV, 167 mV, and 131 mV for 5 mg, 10 mg, and 15 mg respectively. Among all the catalysts the one containing 15 mg of Cu-BTC shows the least over potential of 131 mV. This increase in the activity of the catalyst is because of the synergistic behavior of the hybrid material in which the properties of both the material combine and result in enhanced activity. In Cu-BTC, Cu metal corners are present which are attached to 4 oxygen atoms and form BTC linkers along with square planar vertexes and open metal sites. Because of these metal sites, this material shows high conductivity and results in high adsorption of hydrogen molecules. Although g-C₃N₄ has low active sites yet they exhibit excellent activity by making its hybrids with other catalyst have larger surface area like MOFs. This can be seen from the HER results of the hybrids. The fact that hybrids have better activity can be confirmed by the values of the Tafel slopes of all the fabricated catalysts. From the literature, the catalyst having a low Tafel slope will possess good stability that the one having a high Tafel slope. The Tafel slope of the prepared samples has been determined using the following equation.

$$\eta = c \log j + \alpha \quad (9)$$

Here, η is overpotential,

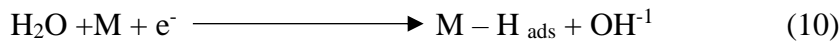
c is Tafel slope,

α = Tafel constant,

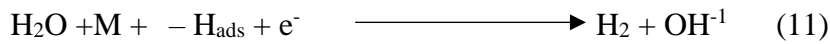
j =current density.

The Tafel slope of pure Cu-BTC and pure g-C₃N₄ is found using the above equation (132 mV/dec), and (153 mV/dec). Similarly, the Tafel slope of the hybrids 5 mg, 10 mg, and 15 mg of Cu-BTC are (86 mV/dec), (98 mV/dec), (59 mV/dec). The Tafel slope for HER can be seen in Figure 14(c). As catalysts having 15 mg of Cu-BTC have low Tafel slope as compared to all other catalysts which confirmed that this hybrid has better activity. From the Tafel slope, no value is less than 39 mV/dec so Volmer and Heyrovsky reaction mechanism is followed for the hydrogen evolution reaction. The mechanism is as follows.

Volmer step:



Heyrovsky step:



The sign 'M' represents the adsorption sites. The discharge of H₂O molecules on the surface of the catalyst in the alkaline medium leads to the formation of a precursor of adsorbed hydrogen.

Figure 14 (b) is the linear sweep voltammetry curves of the prepared catalysts for the oxygen evolution reaction. The figure for OER Cu-BTC and pure g-C₃N₄ gives an overpotential of 330 mV and 324 mV at 10 mA/cm² current density in the alkaline electrolyte solution. At the same current density in the same electrolyte solution, the hybrid of these catalysts shows an overpotential of 247 mV, 238 mV, and 185 mV for 5 mg, 10 mg, and 15 mg g-C₃N₄ in Cu-BTC respectively. for OER again we can see that by increasing the amount of Cu-BTC MOF in graphitic carbon nitride the activity of the hybrids increases gradually. The highest activity can be seen for hybrid having 15 mg of g-C₃N₄ in Cu-BTC, so it follows the same trend as that of HER. The enhancement in catalytic activity in the hybrids is again because of the synergistic effects of both materials present in the hybrid.

The Tafel slope of pure Cu-BTC and pure g-C₃N₄ for OER are (146 mV/dec), and (122 mV/dec) respectively. The Tafel slope of the hybrids containing 5 mg, 10 mg, and 15 mg of g-C₃N₄ in Cu-BTC are (72 mV/dec), (89 mV/dec), and (53 mV/dec) respectively. As the Tafel slope of the hybrid containing 15 mg of Cu-BTC is low as compared to the other hybrids so it confirmed that this hybrid has greater activity among all the prepared samples. For Oxygen evolution reaction irrespective of the values of Tafel slope a 4-electron mechanism is used and completed in 4 steps.

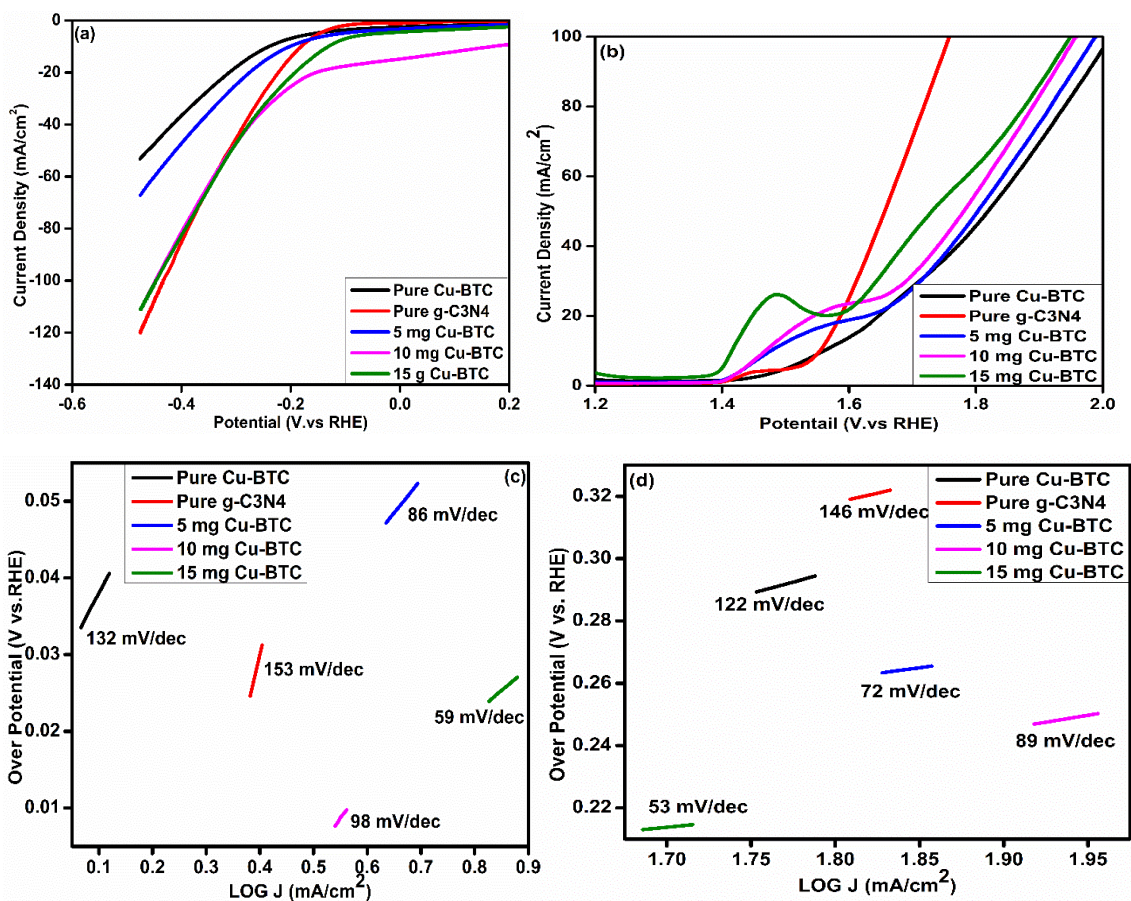


Figure 14: (a, b) HER and OER of the prepared samples, (c,d) Tafel slopes of HER and OER of the prepared samples respectively.

4.4.2 Cyclic Voltammetry (CV) and Electrochemical Impedance Spectroscopy (EIS)

One of the important parameters in determining the activity of a catalyst is the cyclic voltammetry (CV). From the curve of a CV, one can find out the redox reaction and electrochemically active surface area of a catalyst. Figure 15 (a) shows the cyclic voltammetry curve of the prepared catalyst. From the figure, redox reactions are taking

place in all the curves. The upper peak is the peak of oxidation where oxidation takes place and oxygen is produced while the lower peak is the peak of reduction and where hydrogen production takes place. From this CV curve, electrochemical active surface area (ECSA) is determined using origin software. From the graph, it can be seen visually that hybrid has 15 mg of g-C₃N₄ in Cu-BTC which confirms that the activity of this hybrid is high as compared to all other prepared hybrids. The electrochemical active surface area of all the prepared catalysts is given in the table below as can be seen that the catalyst having 15 mg of g-C₃N₄ in Cu-BTC possesses the highest area of 3187 cm². Due to this high area, the active sites available for hydrogen deposition are more and as a result, hydrogen is produced as compared to all other fabricated catalysts hence this is our best catalyst in terms of activity. To further find out the resistances that can slow down the process of hydrogen production electrochemical impedance spectroscopy has been performed. The test is performed in a frequency range of 0.001 KHz to 200 KHz in a 1 molar KOH electrolyte solution. The catalyst which offers the least resistance will have a high yield of hydrogen production so as the activity. Figure 15 (b) shows the EIS of the catalyst synthesized along the analogs circuit. The real resistance is given on the X-axis and the imaginary resistance is given on the Y-axis. From the figure, the catalyst having 15 mg Cu-BTC shows the minimum charge transfer resistance and can be confirmed in Table 3 also. R_p is the polarization resistance it is the resistance offered by the electrolyte solution while R_{ct} is the charge transfer resistance which is the resistance within the catalyst.

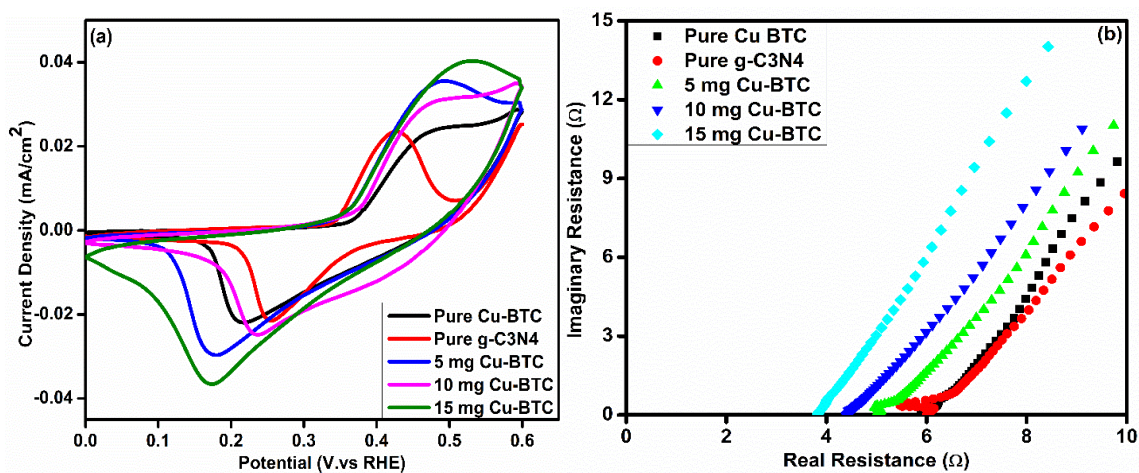


Figure 15: (a) CV curves of all the catalysts, (b) EIS of the prepared Catalysts.

Table 3: EIS summary of Prepared Catalysts

Catalyst	Rp	Rct	ECSA
Pure Cu-BTC	5.98	0.589	2569.43
Pure g-C3N4	2.78	6.44	1976.846
5 mg Cu-BTC/ g-C3N4	5.03	0.745	2938.69
10 mg Cu-BTC/ g-C3N4	4.42	0.966	2892.714
15 mg Cu-BTC/ g-C3N4	4.43	0.240	3187.239

4.4.3 Chronopotentiometry

One of the important parameters to study the activity of a catalyst is to find out its stability using chrono potentiometry or through CV cycles. A Chrono potentiometry test is performed to find out the stability of our best catalyst with exceptional HER and OER activity for 18 h. From the figure, we can see that the stability of the catalyst remains constant and did not drop from the starting value which confirms that the catalyst having 15 mg of Cu-BTC have outstanding stability. This stability is due to the structural properties of the catalyst.

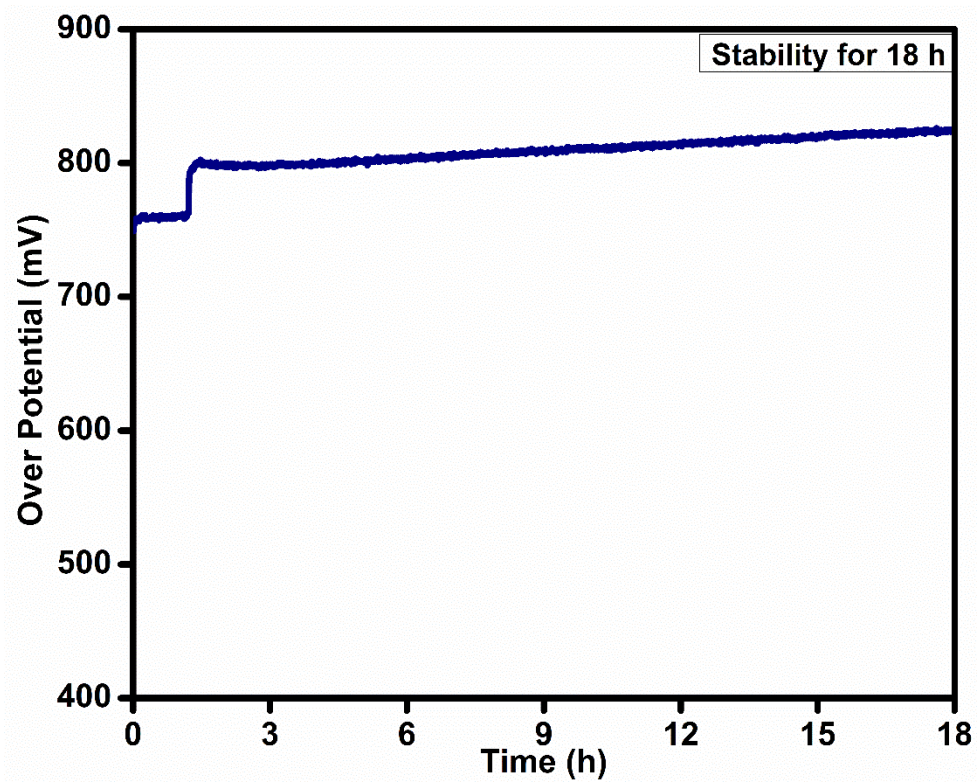


Figure 16: Chrono of the catalyst for 18 h

Conclusions

This research details Cu-BTC electrocatalyst with g-C₃N₄ substrates for the HER in an alkaline medium. We are especially interested in improving electrochemical performance and methods for increasing HER activity. The improved Cu-BTC/ g-C₃N₄ electrocatalyst exhibits excellent performance for HER in an alkaline solution, with an overpotential of 131 mV and a Tafel slope of 59 mV/dec at $j=10$ mA/cm². By using rational g-C₃N₄ as support for Cu-BTC electrocatalysts, it is possible to modify the properties of Cu-BTC -based HER catalysts. Furthermore, this method applies to most known Cu-BTC -based electrocatalysts, including Slinides, carbides, graphic oxides, double-layer hydroxides, etc. The exceptional performance is attributed to the addition of g-C₃N₄ in Cu-BTC hybrids resulting in (1) clumping prevention of pure Cu-BTC electrocatalyst; (2) increasing electronic conductivity; (3) easing the diffusion of the electrolyte and the gas produced; and (4) improving the catalysts' long-term durability. Such findings offer a new avenue for the rational design of Cu-BTC substrate hybrid catalysts for improved water-splitting applications. Cu-BTC-based materials are the most potentially suitable for replacing the expensive but prevalent Pt-based catalysts. This is due to the fact that Cu-BTC-based materials possess a higher HER catalytic activity and are stable throughout a wide pH range. Cu-BTC is an excellent material for use in electrocatalytic applications and processes due to its low overpotential, porosity, stability, affordability, abundance, compatibility, and permeability. The relationship between composition/structure and electrocatalytic performance is the primary emphasis of this article. In addition to covering preparation methods and strategies for improving catalytic activity, the study zeroes in on this relationship. Following significant study and development, all Cu-BTC-based electrocatalysts now available exhibit good behavior when exposed to acidic electrolytes. The perfect catalyst would have a high hydrogen adsorption energy together with a large number of active sites and excellent electrical conductivity.

Recommendation

The electrochemical water-splitting potential of hybrid Cu/BTC catalysts is quite promising. There are still major obstacles to overcome before this technology can be considered practical and cost-effective. Some of these challenges include the research and development of catalysts that are more effective and durable, less expensive to produce, more scalable, able to function in a wider variety of situations, and compatible with renewable energy sources.

More research and development are necessary, but hybrids based on the Cu-BTC catalyst show promise for the future of renewable energy. Research that could be done to improve Cu-BTC catalyst-based hybrids for electrochemical water splitting includes studying the effect of different metal ions on the catalytic activity of Cu-BTC, developing new methods for synthesizing Cu-BTC with improved properties, designing new hybrid materials that combine the advantages of Cu-BTC with other materials, such as metal nanoparticles or carbon nanotubes, and testing Cu-BTC catalysts in different water conditions.

If these issues could be resolved, Cu-BTC catalyst hybrids would become a more appealing option for creating clean energy.

References

- [1] Y. Liu *et al.*, “Metal sulfide/MOF-based composites as visible-light-driven photocatalysts for enhanced hydrogen production from water splitting,” *Coord. Chem. Rev.*, vol. 409, p. 213220, 2020, doi: <https://doi.org/10.1016/j.ccr.2020.213220>.
- [2] M. A. Rasool *et al.*, “An Insight into Carbon Nanomaterial-Based Photocatalytic Water Splitting for Green Hydrogen Production,” *Catalysts*, vol. 13, no. 1. 2023, doi: 10.3390/catal13010066.
- [3] M. Ali, E. Pervaiz, T. Noor, O. Rabi, R. Zahra, and M. Yang, “Recent advancements in MOF-based catalysts for applications in electrochemical and photoelectrochemical water splitting: A review,” *Int. J. Energy Res.*, vol. 45, no. 2, pp. 1190–1226, Feb. 2021, doi: <https://doi.org/10.1002/er.5807>.
- [4] J. Joy, J. Mathew, and S. C. George, “Nanomaterials for photoelectrochemical water splitting – review,” *Int. J. Hydrogen Energy*, vol. 43, no. 10, pp. 4804–4817, 2018, doi: <https://doi.org/10.1016/j.ijhydene.2018.01.099>.
- [5] M. Mehrpooya and R. Habibi, “A review on hydrogen production thermochemical water-splitting cycles,” *J. Clean. Prod.*, vol. 275, p. 123836, 2020, doi: <https://doi.org/10.1016/j.jclepro.2020.123836>.
- [6] U. Sohail, E. Pervaiz, M. Ali, R. Khosa, A. Shakoor, and U. Abdullah, “Role of tungsten carbide (WC) and its hybrids in electrochemical water splitting application-A comprehensive review,” *FlatChem*, p. 100404, 2022.
- [7] R. Khosa, E. Pervaiz, U. Abdullah, M. Ali, U. Sohail, and A. Shakoor, “An Insight on Molybdenum Phosphide and its Hybrids as Catalyst for Electrochemical Water splitting: A Mini-Review,” *Mol. Catal.*, vol. 528, p. 112514, 2022.
- [8] N. Fajrina and M. Tahir, “A critical review in strategies to improve photocatalytic water splitting towards hydrogen production,” *Int. J. Hydrogen Energy*, vol. 44, no. 2, pp. 540–577, 2019, doi: <https://doi.org/10.1016/j.ijhydene.2018.10.200>.

- [9] W. Chen *et al.*, “A review on the visible light active modified photocatalysts for water splitting for hydrogen production,” *Int. J. Energy Res.*, vol. 46, no. 5, pp. 5467–5477, 2022.
- [10] G. Kumar *et al.*, “Biomass based hydrogen production by dark fermentation—recent trends and opportunities for greener processes,” *Curr. Opin. Biotechnol.*, vol. 50, pp. 136–145, 2018, doi: <https://doi.org/10.1016/j.copbio.2017.12.024>.
- [11] Z. Y. Hitit, C. Zampol Lazaro, and P. C. Hallenbeck, “Increased hydrogen yield and COD removal from starch/glucose based medium by sequential dark and photo-fermentation using *Clostridium butyricum* and *Rhodospseudomonas palustris*,” *Int. J. Hydrogen Energy*, vol. 42, no. 30, pp. 18832–18843, 2017, doi: <https://doi.org/10.1016/j.ijhydene.2017.05.161>.
- [12] D. Saadetnejad and R. Yildirim, “Photocatalytic hydrogen production by water splitting over Au/Al-SrTiO₃,” *Int. J. Hydrogen Energy*, vol. 43, no. 2, pp. 1116–1122, 2018, doi: <https://doi.org/10.1016/j.ijhydene.2017.10.154>.
- [13] E. B. Agyekum, C. Nutakor, A. M. Agwa, and S. Kamel, “A critical review of renewable hydrogen production methods: factors affecting their scale-up and its role in future energy generation,” *Membranes (Basel)*, vol. 12, no. 2, p. 173, 2022.
- [14] S. Singla, S. Sharma, S. Basu, N. P. Shetti, and T. M. Aminabhavi, “Photocatalytic water splitting hydrogen production via environmental benign carbon based nanomaterials,” *Int. J. Hydrogen Energy*, vol. 46, no. 68, pp. 33696–33717, 2021, doi: <https://doi.org/10.1016/j.ijhydene.2021.07.187>.
- [15] M. Amin *et al.*, “Hydrogen production through renewable and non-renewable energy processes and their impact on climate change,” *Int. J. Hydrogen Energy*, 2022.
- [16] H. Ishaq, I. Dincer, and C. Crawford, “A review on hydrogen production and utilization: Challenges and opportunities,” *Int. J. Hydrogen Energy*, vol. 47, no. 62, pp. 26238–26264, 2022.

- [17] R. Solanki *et al.*, “Investigation of recent progress in metal-based materials as catalysts toward electrochemical water splitting,” *J. Environ. Chem. Eng.*, vol. 10, no. 4, p. 108207, 2022, doi: <https://doi.org/10.1016/j.jece.2022.108207>.
- [18] F. Safari and I. Dincer, “A review and comparative evaluation of thermochemical water splitting cycles for hydrogen production,” *Energy Convers. Manag.*, vol. 205, p. 112182, 2020.
- [19] X. Chen and W. Shangguan, “Hydrogen production from water splitting on CdS-based photocatalysts using solar light,” *Front. Energy*, vol. 7, no. 1, pp. 111–118, 2013, doi: 10.1007/s11708-012-0228-4.
- [20] J. Zhang, Q. Zhang, and X. Feng, “Support and Interface Effects in Water-Splitting Electrocatalysts,” *Adv. Mater.*, vol. 31, no. 31, p. 1808167, 2019, doi: <https://doi.org/10.1002/adma.201808167>.
- [21] B. You and Y. Sun, “Innovative Strategies for Electrocatalytic Water Splitting,” *Acc. Chem. Res.*, vol. 51, no. 7, pp. 1571–1580, Jul. 2018, doi: 10.1021/acs.accounts.8b00002.
- [22] A. Wu *et al.*, “Integrating the active OER and HER components as the heterostructures for the efficient overall water splitting,” *Nano Energy*, vol. 44, pp. 353–363, 2018, doi: <https://doi.org/10.1016/j.nanoen.2017.11.045>.
- [23] W. Fang *et al.*, “Metal-organic framework derived Fe-Co-CN/reduced graphene oxide for efficient HER and OER,” *Electrochim. Acta*, vol. 365, p. 137384, 2021, doi: <https://doi.org/10.1016/j.electacta.2020.137384>.
- [24] J. E. Lee *et al.*, “Mini review on H₂ production from electrochemical water splitting according to special nanostructured morphology of electrocatalysts,” *Fuel*, vol. 308, p. 122048, 2022.
- [25] B. T. Jebaslinhepzybai, T. Partheeban, D. S. Gavali, R. Thapa, and M. Sasidharan, “One-pot solvothermal synthesis of Co₂P nanoparticles: An efficient HER and OER electrocatalysts,” *Int. J. Hydrogen Energy*, vol. 46, no. 42, pp. 21924–21938, 2021, doi: <https://doi.org/10.1016/j.ijhydene.2021.04.022>.

- [26] S. Tan, W. Ouyang, Y. Ji, and Q. Hong, “Carbon wrapped bimetallic NiCo nanospheres toward excellent HER and OER performance,” *J. Alloys Compd.*, vol. 889, p. 161528, 2021, doi: <https://doi.org/10.1016/j.jallcom.2021.161528>.
- [27] N. H. Alf, H. O. S. Crystal, R. Kripal, and L. C. Shukla, “Theoretical Zero Field Splitting Parameters of Fe 3 + doped,” vol. 10, no. 1, pp. 5–9, 2022.
- [28] S. Roy *et al.*, “Mechanistic insights into the promotional effect of Ni substitution in non-noble metal carbides for highly enhanced water splitting,” *Appl. Catal. B Environ.*, vol. 298, p. 120560, 2021, doi: <https://doi.org/10.1016/j.apcatb.2021.120560>.
- [29] B. Zhang *et al.*, “Designing MOF Nanoarchitectures for Electrochemical Water Splitting,” *Adv. Mater.*, vol. 33, no. 17, p. 2006042, Apr. 2021, doi: <https://doi.org/10.1002/adma.202006042>.
- [30] D. Senthil Raja, X.-F. Chuah, and S.-Y. Lu, “In Situ Grown Bimetallic MOF-Based Composite as Highly Efficient Bifunctional Electrocatalyst for Overall Water Splitting with Ultrastability at High Current Densities,” *Adv. Energy Mater.*, vol. 8, no. 23, p. 1801065, Aug. 2018, doi: <https://doi.org/10.1002/aenm.201801065>.
- [31] T. Ishaq *et al.*, “A perspective on possible amendments in semiconductors for enhanced photocatalytic hydrogen generation by water splitting,” *Int. J. Hydrogen Energy*, vol. 46, no. 79, pp. 39036–39057, 2021, doi: <https://doi.org/10.1016/j.ijhydene.2021.09.165>.
- [32] W. Wang, X. Xu, W. Zhou, and Z. Shao, “Recent Progress in Metal-Organic Frameworks for Applications in Electrocatalytic and Photocatalytic Water Splitting,” *Adv. Sci.*, vol. 4, no. 4, p. 1600371, Apr. 2017, doi: <https://doi.org/10.1002/advs.201600371>.
- [33] Y. Fang, Y. Ma, M. Zheng, P. Yang, A. M. Asiri, and X. Wang, “Metal–organic frameworks for solar energy conversion by photoredox catalysis,” *Coord. Chem. Rev.*, vol. 373, pp. 83–115, 2018, doi: <https://doi.org/10.1016/j.ccr.2017.09.013>.

- [34] M. Ni, M. K. H. Leung, D. Y. C. Leung, and K. Sumathy, "A review and recent developments in photocatalytic water-splitting using TiO₂ for hydrogen production," *Renew. Sustain. Energy Rev.*, vol. 11, no. 3, pp. 401–425, 2007, doi: <https://doi.org/10.1016/j.rser.2005.01.009>.
- [35] Y. Zhang, S. Yuan, G. Day, X. Wang, X. Yang, and H.-C. Zhou, "Luminescent sensors based on metal-organic frameworks," *Coord. Chem. Rev.*, vol. 354, pp. 28–45, 2018, doi: <https://doi.org/10.1016/j.ccr.2017.06.007>.
- [36] H. Li, K. Wang, Y. Sun, C. T. Lollar, J. Li, and H.-C. Zhou, "Recent advances in gas storage and separation using metal-organic frameworks," *Mater. Today*, vol. 21, no. 2, pp. 108–121, 2018, doi: <https://doi.org/10.1016/j.mattod.2017.07.006>.
- [37] H. M. El-Bery and H. N. Abdelhamid, "Photocatalytic hydrogen generation via water splitting using ZIF-67 derived Co₃O₄@C/TiO₂," *J. Environ. Chem. Eng.*, vol. 9, no. 4, p. 105702, 2021, doi: <https://doi.org/10.1016/j.jece.2021.105702>.
- [38] A. R. Abbasi, M. Karimi, and K. Daasbjerg, "Efficient removal of crystal violet and methylene blue from wastewater by ultrasound nanoparticles Cu-MOF in comparison with mechanochemistry method," *Ultrason. Sonochem.*, vol. 37, pp. 182–191, 2017, doi: <https://doi.org/10.1016/j.ultsonch.2017.01.007>.
- [39] B. Wei, J. Wu, G. Mei, Z. Qi, W. Hu, and Z. Wang, "NiCo₂O₄ nanowire arrays rich in oxygen deficiencies for hydrogen evolution reaction," *Int. J. Hydrogen Energy*, vol. 44, no. 13, pp. 6612–6617, 2019, doi: <https://doi.org/10.1016/j.ijhydene.2019.01.183>.
- [40] A. Roy, D. Hursán, K. Artyushkova, P. Atanassov, C. Janáky, and A. Serov, "Nanostructured metal-N-C electrocatalysts for CO₂ reduction and hydrogen evolution reactions," *Appl. Catal. B Environ.*, vol. 232, pp. 512–520, 2018, doi: <https://doi.org/10.1016/j.apcatb.2018.03.093>.
- [41] J. Song, X. Gu, J. Cheng, N. Fan, H. Zhang, and H. Su, "Remarkably boosting catalytic H₂ evolution from ammonia borane through the visible-light-driven synergistic electron effect of non-plasmonic noble-metal-free nanoparticles and photoactive metal-organic frameworks," *Appl. Catal. B Environ.*, vol. 225, pp.

424–432, 2018, doi: <https://doi.org/10.1016/j.apcatb.2017.12.024>.

- [42] R. Nivetha *et al.*, “Cu based Metal Organic Framework (Cu-MOF) for electrocatalytic hydrogen evolution reaction,” *Mater. Res. Express*, vol. 7, no. 11, 2020, doi: 10.1088/2053-1591/abb056.
- [43] W. Hong *et al.*, “Self-supported nanoporous cobalt phosphosulfate electrodes for efficient hydrogen evolution reaction,” *Appl. Catal. B Environ.*, vol. 251, pp. 213–219, 2019, doi: <https://doi.org/10.1016/j.apcatb.2019.03.070>.
- [44] T. Song *et al.*, “Stable and improved visible-light photocatalytic hydrogen evolution using copper(ii)–organic frameworks: engineering the crystal structures,” *J. Mater. Chem. A*, vol. 5, no. 13, pp. 6013–6018, 2017, doi: 10.1039/C7TA00095B.
- [45] R. Gupta, J. Shah, R. Singh, and R. K. Kotnala, “Nonphotocatalytic Water Splitting Process to Generate Green Electricity in Alkali Doped Zinc Oxide Based Hydroelectric Cell,” *Energy & Fuels*, vol. 35, no. 11, pp. 9714–9726, Jun. 2021, doi: 10.1021/acs.energyfuels.1c01164.
- [46] H. L. Nguyen, “Metal–organic frameworks for photocatalytic water splitting,” *Sol. RRL*, vol. 5, no. 7, p. 2100198, 2021.
- [47] S. Liu, Y.-J. Lei, Z.-J. Xin, Y.-B. Lu, and H.-Y. Wang, “Water splitting based on homogeneous copper molecular catalysts,” *J. Photochem. Photobiol. A Chem.*, vol. 355, pp. 141–151, 2018, doi: <https://doi.org/10.1016/j.jphotochem.2017.09.060>.
- [48] H. Tong, S. Ouyang, Y. Bi, N. Umezawa, M. Oshikiri, and J. Ye, “Nano-photocatalytic Materials: Possibilities and Challenges,” *Adv. Mater.*, vol. 24, no. 2, pp. 229–251, Jan. 2012, doi: <https://doi.org/10.1002/adma.201102752>.
- [49] P. Jiménez-Calvo, V. Caps, and V. Keller, “Plasmonic Au-based junctions onto TiO₂, gC₃N₄, and TiO₂-gC₃N₄ systems for photocatalytic hydrogen production: Fundamentals and challenges,” *Renew. Sustain. Energy Rev.*, vol. 149, p. 111095, 2021.

- [50] X. Chen, S. Shen, L. Guo, and S. S. Mao, "Semiconductor-based Photocatalytic Hydrogen Generation," *Chem. Rev.*, vol. 110, no. 11, pp. 6503–6570, Nov. 2010, doi: 10.1021/cr1001645.
- [51] M. Javed *et al.*, "Synthesis, characterization and photocatalytic applications of s-doped graphitic carbon nitride nanocomposites with nickel doped zinc oxide nanoparticles," *Dig. J. Nanomater. Biostructures*, vol. 15, no. 4, pp. 1097–1105, 2020.
- [52] A. A. Ismail and D. W. Bahnemann, "Photochemical splitting of water for hydrogen production by photocatalysis: A review," *Sol. Energy Mater. Sol. Cells*, vol. 128, pp. 85–101, 2014, doi: <https://doi.org/10.1016/j.solmat.2014.04.037>.
- [53] S. Z. Islam, A. Reed, N. Wanninayake, D. Y. Kim, and S. E. Rankin, "Remarkable Enhancement of Photocatalytic Water Oxidation in N₂/Ar Plasma Treated, Mesoporous TiO₂ Films," *J. Phys. Chem. C*, vol. 120, no. 26, pp. 14069–14081, Jul. 2016, doi: 10.1021/acs.jpcc.6b02622.
- [54] B. H. Nguyen and V. H. Nguyen, "Recent advances in research on plasmonic enhancement of photocatalysis," *Adv. Nat. Sci. Nanosci. Nanotechnol.*, vol. 6, no. 4, p. 43001, 2015, doi: 10.1088/2043-6262/6/4/043001.
- [55] R. Shwetharani, M. Sakar, H. R. Chandan, and R. Geetha Balakrishna, "Observation of simultaneous photocatalytic degradation and hydrogen evolution on the lanthanum modified TiO₂ nanostructures," *Mater. Lett.*, vol. 218, pp. 262–265, 2018, doi: <https://doi.org/10.1016/j.matlet.2018.02.031>.
- [56] J. C. Moore, R. Louder, and C. V Thompson, "Photocatalytic Activity and Stability of Porous Polycrystalline ZnO Thin-Films Grown via a Two-Step Thermal Oxidation Process," *Coatings*, vol. 4, no. 3, 2014, doi: 10.3390/coatings4030651.
- [57] A. Kudo and Y. Miseki, "Heterogeneous photocatalyst materials for water splitting," *Chem. Soc. Rev.*, vol. 38, no. 1, pp. 253–278, 2009.
- [58] R. M. Navarro Yerga, M. C. Alvarez Galvan, F. Del Valle, J. A. Villoria de la

- Mano, and J. L. G. Fierro, "Water splitting on semiconductor catalysts under visible-light irradiation," *ChemSusChem Chem. Sustain. Energy Mater.*, vol. 2, no. 6, pp. 471–485, 2009.
- [59] Y. Xu, M. Kraft, and R. Xu, "Metal-free carbonaceous electrocatalysts and photocatalysts for water splitting," *Chem. Soc. Rev.*, vol. 45, no. 11, pp. 3039–3052, 2016.
- [60] T. Jafari, E. Moharreri, A. S. Amin, R. Miao, W. Song, and S. L. Suib, "Photocatalytic Water Splitting—The Untamed Dream: A Review of Recent Advances," *Molecules*, vol. 21, no. 7, 2016, doi: 10.3390/molecules21070900.
- [61] Y. Liu, Y.-Y. Deng, Q. Zhang, and H. Liu, "Overview of recent developments of resource recovery from wastewater via electrochemistry-based technologies," *Sci. Total Environ.*, vol. 757, p. 143901, 2021.
- [62] L. Zhang *et al.*, "Recent advances in 1D electrospun nanocatalysts for electrochemical water splitting," *Small Struct.*, vol. 2, no. 2, p. 2000048, 2021.
- [63] Y. Wang, B. Kong, D. Zhao, H. Wang, and C. Selomulya, "Strategies for developing transition metal phosphides as heterogeneous electrocatalysts for water splitting," *Nano Today*, vol. 15, pp. 26–55, 2017, doi: <https://doi.org/10.1016/j.nantod.2017.06.006>.
- [64] B. You, M. T. Tang, C. Tsai, F. Abild-Pedersen, X. Zheng, and H. Li, "Enhancing Electrocatalytic Water Splitting by Strain Engineering," *Adv. Mater.*, vol. 31, no. 17, p. 1807001, Apr. 2019, doi: <https://doi.org/10.1002/adma.201807001>.
- [65] B. You and Y. Sun, "Hierarchically porous nickel sulfide multifunctional superstructures," *Adv. Energy Mater.*, vol. 6, no. 7, p. 1502333, 2016.
- [66] B. M. Hunter, H. B. Gray, and A. M. Muller, "Earth-abundant heterogeneous water oxidation catalysts," *Chem. Rev.*, vol. 116, no. 22, pp. 14120–14136, 2016.
- [67] B. You *et al.*, "Universal surface engineering of transition metals for superior electrocatalytic hydrogen evolution in neutral water," *J. Am. Chem. Soc.*, vol. 139, no. 35, pp. 12283–12290, 2017.

- [68] C. Chen *et al.*, “Highly crystalline multimetallic nanoframes with three-dimensional electrocatalytic surfaces,” *Science* (80-.), vol. 343, no. 6177, pp. 1339–1343, 2014.
- [69] G. Liu *et al.*, “Promoting active species generation by plasmon-induced hot-electron excitation for efficient electrocatalytic oxygen evolution,” *J. Am. Chem. Soc.*, vol. 138, no. 29, pp. 9128–9136, 2016.
- [70] C. G. Morales-Guio, L.-A. Stern, and X. Hu, “Nanostructured hydrotreating catalysts for electrochemical hydrogen evolution,” *Chem. Soc. Rev.*, vol. 43, no. 18, pp. 6555–6569, 2014.
- [71] Y. Guo *et al.*, “Nanoarchitectonics for transition-metal-sulfide-based electrocatalysts for water splitting,” *Adv. Mater.*, vol. 31, no. 17, p. 1807134, 2019.
- [72] Y. Yan, B. Y. Xia, B. Zhao, and X. Wang, “A review on noble-metal-free bifunctional heterogeneous catalysts for overall electrochemical water splitting,” *J. Mater. Chem. A*, vol. 4, no. 45, pp. 17587–17603, 2016.
- [73] R. Paul, L. Zhu, H. Chen, J. Qu, and L. Dai, “Recent advances in carbon-based metal-free electrocatalysts,” *Adv. Mater.*, vol. 31, no. 31, p. 1806403, 2019.
- [74] J. R. McKone, S. C. Marinescu, B. S. Brunschwig, J. R. Winkler, and H. B. Gray, “Earth-abundant hydrogen evolution electrocatalysts,” *Chem. Sci.*, vol. 5, no. 3, pp. 865–878, 2014.
- [75] S. Bae, I. Jeon, J. Mahmood, and J. Baek, “Molybdenum-Based Carbon Hybrid Materials to Enhance the Hydrogen Evolution Reaction,” *Chem. Eur. J.*, vol. 24, no. 69, pp. 18158–18179, 2018.
- [76] W. Zhou *et al.*, “Recent developments of carbon-based electrocatalysts for hydrogen evolution reaction,” *Nano Energy*, vol. 28, pp. 29–43, 2016.
- [77] R. Wang, J. Han, X. Zhang, and B. Song, “Synergistic modulation in MX₂ (where M= Mo or W or V, and X= S or Se) for an enhanced hydrogen evolution reaction,” *J. Mater. Chem. A*, vol. 6, no. 44, pp. 21847–21858, 2018.

- [78] X. Hou, Y. Li, L. Cheng, X. Feng, H. Zhang, and S. Han, "Cobalt-molybdenum disulfide supported on nitrogen-doped graphene towards an efficient hydrogen evolution reaction," *Int. J. Hydrogen Energy*, vol. 44, no. 23, pp. 11664–11674, 2019.
- [79] C. He, T. Bo, B. Wang, and J. Tao, "RGO induced one-dimensional bimetallic carbide nanorods: An efficient and pH-universal hydrogen evolution reaction electrocatalyst," *Nano Energy*, vol. 62, pp. 85–93, 2019.
- [80] W. Li, B. Yu, Y. Hu, X. Wang, D. Yang, and Y. Chen, "Core-shell structure of NiSe₂ nanoparticles@ nitrogen-doped graphene for hydrogen evolution reaction in both acidic and alkaline media," *ACS Sustain. Chem. Eng.*, vol. 7, no. 4, pp. 4351–4359, 2019.
- [81] J. Ma *et al.*, "Polyaniline derived N-doped carbon-coated cobalt phosphide nanoparticles deposited on N-doped graphene as an efficient electrocatalyst for hydrogen evolution reaction," *Small*, vol. 14, no. 2, p. 1702895, 2018.
- [82] W. Chen *et al.*, "Tungsten carbide-nitride on graphene nanoplatelets as a durable hydrogen evolution electrocatalyst," *ChemSusChem*, vol. 7, no. 9, pp. 2414–2418, 2014.
- [83] X. Liu *et al.*, "Metal (Ni, Co)-metal oxides/graphene nanocomposites as multifunctional electrocatalysts," *Adv. Funct. Mater.*, vol. 25, no. 36, pp. 5799–5808, 2015.
- [84] A. Ali and P. K. Shen, "Nonprecious metal's graphene-supported electrocatalysts for hydrogen evolution reaction: Fundamentals to applications," *Carbon Energy*, vol. 2, no. 1, pp. 99–121, Mar. 2020, doi: <https://doi.org/10.1002/cey2.26>.
- [85] F. Safizadeh, E. Ghali, and G. Houlachi, "Electrocatalysis developments for hydrogen evolution reaction in alkaline solutions—a review," *Int. J. Hydrogen Energy*, vol. 40, no. 1, pp. 256–274, 2015.
- [86] R. Kirpal, "pdf_paper_view @ isroset.org." 2022, [Online]. Available: https://isroset.org/pdf_paper_view.php?paper_id=2890&4-ISROSET-IJSRPAS-

07965.pdf.

- [87] M. Ďurovič, J. Hnát, and K. Bouzek, “Electrocatalysts for the hydrogen evolution reaction in alkaline and neutral media. A comparative review,” *J. Power Sources*, vol. 493, p. 229708, 2021, doi: <https://doi.org/10.1016/j.jpowsour.2021.229708>.
- [88] J. Wang *et al.*, “Earth-abundant transition-metal-based bifunctional catalysts for overall electrochemical water splitting: A review,” *J. Alloys Compd.*, vol. 819, p. 153346, 2020, doi: <https://doi.org/10.1016/j.jallcom.2019.153346>.
- [89] H. Furukawa, K. E. Cordova, M. O’Keeffe, and O. M. Yaghi, “The chemistry and applications of metal-organic frameworks,” *Science (80-.)*, vol. 341, no. 6149, p. 1230444, 2013.
- [90] C. R. Kim, T. Uemura, and S. Kitagawa, “Inorganic nanoparticles in porous coordination polymers,” *Chem. Soc. Rev.*, vol. 45, no. 14, pp. 3828–3845, 2016.
- [91] Z. Wang and S. M. Cohen, “Postsynthetic modification of metal–organic frameworks,” *Chem. Soc. Rev.*, vol. 38, no. 5, pp. 1315–1329, 2009.
- [92] H. Furukawa *et al.*, “Ultrahigh porosity in metal-organic frameworks,” *Science (80-.)*, vol. 329, no. 5990, pp. 424–428, 2010.
- [93] Q. Wang and D. Astruc, “State of the Art and Prospects in Metal–Organic Framework (MOF)-Based and MOF-Derived Nanocatalysis,” *Chem. Rev.*, vol. 120, no. 2, pp. 1438–1511, Jan. 2020, doi: [10.1021/acs.chemrev.9b00223](https://doi.org/10.1021/acs.chemrev.9b00223).
- [94] P. Silva, S. M. F. Vilela, J. P. C. Tome, and F. A. A. Paz, “Multifunctional metal–organic frameworks: from academia to industrial applications,” *Chem. Soc. Rev.*, vol. 44, no. 19, pp. 6774–6803, 2015.
- [95] J. Khan, N. Iqbal, A. Asghar, and T. Noor, “Novel amine functionalized metal organic framework synthesis for enhanced carbon dioxide capture,” *Mater. Res. Express*, vol. 6, no. 10, p. 105539, 2019.
- [96] L. E. Kreno, K. Leong, O. K. Farha, M. Allendorf, R. P. Van Duyne, and J. T. Hupp, “Metal–organic framework materials as chemical sensors,” *Chem. Rev.*,

vol. 112, no. 2, pp. 1105–1125, 2012.

- [97] N. Abdollahi, M. Y. Masoomi, A. Morsali, P. C. Junk, and J. Wang, “Sonochemical synthesis and structural characterization of a new Zn (II) nanoplate metal–organic framework with removal efficiency of Sudan red and Congo red,” *Ultrason. Sonochem.*, vol. 45, pp. 50–56, 2018.
- [98] M. S. Samuel, J. Bhattacharya, C. Parthiban, G. Viswanathan, and N. D. P. Singh, “Ultrasound-assisted synthesis of metal organic framework for the photocatalytic reduction of 4-nitrophenol under direct sunlight,” *Ultrason. Sonochem.*, vol. 49, pp. 215–221, 2018.
- [99] F. Zhang, T. Zhang, X. Zou, X. Liang, G. Zhu, and F. Qu, “Electrochemical synthesis of metal organic framework films with proton conductive property,” *Solid State Ionics*, vol. 301, pp. 125–132, 2017.
- [100] A. Carné-Sánchez, I. Imaz, M. Cano-Sarabia, and D. Maspoch, “A spray-drying strategy for synthesis of nanoscale metal–organic frameworks and their assembly into hollow superstructures,” *Nat. Chem.*, vol. 5, no. 3, pp. 203–211, 2013.
- [101] P. A. Bayliss *et al.*, “Synthesis of metal–organic frameworks by continuous flow,” *Green Chem.*, vol. 16, no. 8, pp. 3796–3802, 2014.
- [102] B. He *et al.*, “Continuous Flow Synthesis of a Zr Magnetic Framework Composite for Post-Combustion CO₂ Capture,” *Chem. Eur. J.*, vol. 25, no. 57, pp. 13184–13188, 2019.
- [103] J. Klinowski, F. A. A. Paz, P. Silva, and J. Rocha, “Microwave-assisted synthesis of metal–organic frameworks,” *Dalt. Trans.*, vol. 40, no. 2, pp. 321–330, 2011.
- [104] A. Huang, L. Wan, and J. Caro, “Microwave-assisted synthesis of well-shaped UiO-66-NH₂ with high CO₂ adsorption capacity,” *Mater. Res. Bull.*, vol. 98, pp. 308–313, 2018.
- [105] S. Rojas-Buzo *et al.*, “Tailoring Lewis/Bronsted acid properties of MOF nodes via hydrothermal and solvothermal synthesis: simple approach with exceptional catalytic implications,” *Chem. Sci.*, vol. 12, no. 29, pp. 10106–10115, 2021.

- [106] Y. Hao, Y. Xu, W. Liu, and X. Sun, "Co/CoP embedded in a hairy nitrogen-doped carbon polyhedron as an advanced tri-functional electrocatalyst," *Mater. Horizons*, vol. 5, no. 1, pp. 108–115, 2018.
- [107] L. Qin, Z. Xu, Y. Zheng, C. Li, J. Mao, and G. Zhang, "Confined Transformation of Organometal-Encapsulated MOFs into Spinel CoFe₂O₄/C Nanocubes for Low-Temperature Catalytic Oxidation," *Adv. Funct. Mater.*, vol. 30, no. 14, p. 1910257, 2020.
- [108] W. Zhou *et al.*, "Improved conductivity of a new Co (II)-MOF by assembled acetylene black for efficient hydrogen evolution reaction," *CrystEngComm*, vol. 20, no. 33, pp. 4804–4809, 2018.
- [109] K. Rui *et al.*, "Direct hybridization of noble metal nanostructures on 2D metal–organic framework nanosheets to catalyze hydrogen evolution," *Nano Lett.*, vol. 19, no. 12, pp. 8447–8453, 2019.
- [110] S. eun Kim and A. Muthurasu, "Metal-organic framework–assisted bimetallic Ni@ Cu microsphere for enzyme-free electrochemical sensing of glucose," *J. Electroanal. Chem.*, vol. 873, p. 114356, 2020.
- [111] Y. H. Budnikova, "Recent advances in metal–organic frameworks for electrocatalytic hydrogen evolution and overall water splitting reactions," *Dalt. Trans.*, vol. 49, no. 36, pp. 12483–12502, 2020.
- [112] M. Nemiwal, V. Gosu, T. C. Zhang, and D. Kumar, "Metal organic frameworks as electrocatalysts: Hydrogen evolution reactions and overall water splitting," *Int. J. Hydrogen Energy*, vol. 46, no. 17, pp. 10216–10238, 2021, doi: <https://doi.org/10.1016/j.ijhydene.2020.12.146>.
- [113] W. Han, M. Li, Y. Ma, and J. Yang, "Cobalt-Based Metal-Organic Frameworks and Their Derivatives for Hydrogen Evolution Reaction ," *Frontiers in Chemistry* , vol. 8. 2020, [Online]. Available: <https://www.frontiersin.org/articles/10.3389/fchem.2020.592915>.
- [114] Z. Fuqin, C. Zhang, G. Xiaohui, C. Du, Z. Zhuang, and W. Chen, "Immobilizing

- Pd nanoclusters into electronically conductive metal-organic frameworks as Bi-functional electrocatalysts for hydrogen evolution and oxygen reduction reactions,” *Electrochim. Acta*, vol. 306, Mar. 2019, doi: 10.1016/j.electacta.2019.03.175.
- [115] H. Yang *et al.*, “General synthetic strategy for libraries of supported multicomponent metal nanoparticles,” *ACS Nano*, vol. 12, no. 5, pp. 4594–4604, 2018.
- [116] X. Dai *et al.*, “Molybdenum polysulfide anchored on porous Zr-metal organic framework to enhance the performance of hydrogen evolution reaction,” *J. Phys. Chem. C*, vol. 120, no. 23, pp. 12539–12548, 2016.
- [117] F. Li, Q. Shao, X. Huang, and J. Lang, “Nanoscale trimetallic metal–organic frameworks enable efficient oxygen evolution electrocatalysis,” *Angew. Chemie*, vol. 130, no. 7, pp. 1906–1910, 2018.
- [118] F. Li *et al.*, “Large-Scale, Bottom-Up Synthesis of Binary Metal–Organic Framework Nanosheets for Efficient Water Oxidation,” *Angew. Chemie*, vol. 131, no. 21, pp. 7125–7130, 2019.
- [119] W. Cheng, H. Zhang, D. Luan, and X. W. Lou, “Exposing unsaturated Cu¹-O₂ sites in nanoscale Cu-MOF for efficient electrocatalytic hydrogen evolution,” *Sci. Adv.*, vol. 7, no. 18, p. eabg2580, 2021.
- [120] M. Wang *et al.*, “Site-Specified Two-Dimensional Heterojunction of Pt Nanoparticles/Metal–Organic Frameworks for Enhanced Hydrogen Evolution,” *J. Am. Chem. Soc.*, vol. 143, no. 40, pp. 16512–16518, 2021.
- [121] Z. Xue *et al.*, “Missing-linker metal-organic frameworks for oxygen evolution reaction,” *Nat. Commun.*, vol. 10, no. 1, pp. 1–8, 2019.
- [122] D. Liu *et al.*, “3D porous Ru-doped NiCo-MOF hollow nanospheres for boosting oxygen evolution reaction electrocatalysis,” *Inorg. Chem.*, vol. 60, no. 8, pp. 5882–5889, 2021.
- [123] X. Zhao *et al.*, “Mixed-node metal–organic frameworks as efficient

- electrocatalysts for oxygen evolution reaction,” *ACS Energy Lett.*, vol. 3, no. 10, pp. 2520–2526, 2018.
- [124] D. S. Raja, H.-W. Lin, and S.-Y. Lu, “Synergistically well-mixed MOFs grown on nickel foam as highly efficient durable bifunctional electrocatalysts for overall water splitting at high current densities,” *Nano Energy*, vol. 57, pp. 1–13, 2019.
- [125] W. Cheng, S. Xi, Z.-P. Wu, D. Luan, and X. W. Lou, “In situ activation of Br-confined Ni-based metal-organic framework hollow prisms toward efficient electrochemical oxygen evolution,” *Sci. Adv.*, vol. 7, no. 46, p. eabk0919, 2021.
- [126] P. Farinazzo Bergamo Dias Martins, P. Papa Lopes, E. A. Ticianelli, V. R. Stamenkovic, N. M. Markovic, and D. Strmcnik, “Hydrogen evolution reaction on copper: Promoting water dissociation by tuning the surface oxophilicity,” *Electrochem. commun.*, vol. 100, pp. 30–33, 2019, doi: <https://doi.org/10.1016/j.elecom.2019.01.006>.
- [127] L. Ye and Z. Wen, “Self-supported three-dimensional Cu/Cu₂O–CuO/rGO nanowire array electrodes for an efficient hydrogen evolution reaction,” *Chem. Commun.*, vol. 54, no. 49, pp. 6388–6391, 2018.
- [128] A. Tahira, Z. H. Ibupoto, M. Willander, and O. Nur, “Advanced Co₃O₄–CuO nano-composite based electrocatalyst for efficient hydrogen evolution reaction in alkaline media,” *Int. J. Hydrogen Energy*, vol. 44, no. 48, pp. 26148–26157, 2019.
- [129] L. Yu *et al.*, “Cu nanowires shelled with NiFe layered double hydroxide nanosheets as bifunctional electrocatalysts for overall water splitting,” *Energy Environ. Sci.*, vol. 10, no. 8, pp. 1820–1827, 2017.
- [130] L. Yu *et al.*, “Hierarchical Cu@CoFe layered double hydroxide core-shell nanoarchitectures as bifunctional electrocatalysts for efficient overall water splitting,” *Nano Energy*, vol. 41, pp. 327–336, 2017.
- [131] Y.-S. Xie, Z. Wang, M. Ju, X. Long, and S. Yang, “Dispersing transition metal vacancies in layered double hydroxides by ionic reductive complexation extraction for efficient water oxidation,” *Chem. Sci.*, vol. 10, no. 36, pp. 8354–

8359, 2019.

- [132] Y. Zheng *et al.*, “Three-dimensional NiCu layered double hydroxide nanosheets array on carbon cloth for enhanced oxygen evolution,” *Electrochim. Acta*, vol. 282, pp. 735–742, 2018.
- [133] S. Hu, Y. Tan, C. Feng, H. Wu, J. Zhang, and H. Mei, “Synthesis of N doped NiZnCu-layered double hydroxides with reduced graphene oxide on nickel foam as versatile electrocatalysts for hydrogen production in hybrid-water electrolysis,” *J. Power Sources*, vol. 453, p. 227872, 2020.
- [134] J. Tian, Q. Liu, N. Cheng, A. M. Asiri, and X. Sun, “Self-supported Cu₃P nanowire arrays as an integrated high-performance three-dimensional cathode for generating hydrogen from water,” *Angew. Chemie*, vol. 126, no. 36, pp. 9731–9735, 2014.
- [135] S. Chu *et al.*, “Holey Ni-Cu phosphide nanosheets as a highly efficient and stable electrocatalyst for hydrogen evolution,” *Appl. Catal. B Environ.*, vol. 243, pp. 537–545, 2019.
- [136] A. Han, H. Zhang, R. Yuan, H. Ji, and P. Du, “Crystalline copper phosphide nanosheets as an efficient janus catalyst for overall water splitting,” *ACS Appl. Mater. Interfaces*, vol. 9, no. 3, pp. 2240–2248, 2017.
- [137] S. Kumaravel, K. Karthick, P. Thiruvengadam, J. M. Johny, S. S. Sankar, and S. Kundu, “Tuning Cu Overvoltage for a Copper–Telluride System in Electrocatalytic Water Reduction and Feasible Feedstock Conversion: A New Approach,” *Inorg. Chem.*, vol. 59, no. 15, pp. 11129–11141, 2020.
- [138] K. C. Majhi and M. Yadav, “Transition metal chalcogenides based nanocomposites as efficient electrocatalyst for hydrogen evolution reaction over the entire pH range,” *Int. J. Hydrogen Energy*, vol. 45, no. 46, pp. 24219–24231, 2020.
- [139] K. Yang *et al.*, “Ultrasmall Ru/Cu-doped RuO₂ Complex Embedded in Amorphous Carbon Skeleton as Highly Active Bifunctional Electrocatalysts for

Overall Water Splitting,” *Small*, vol. 14, no. 41, p. 1803009, Oct. 2018, doi: <https://doi.org/10.1002/sml.201803009>.

- [140] X. Huang, “Channel Rich RuCu Nanosheets for pH-Universal Overall Water Splitting Electrocatalysis,” *Angew. Chemie Int. Ed.*, vol. 58, Jul. 2019, doi: 10.1002/anie.201908092.
- [141] M. Yang *et al.*, “Conversion of bimetallic MOF to Ru-doped Cu electrocatalysts for efficient hydrogen evolution in alkaline media,” *Sci. Bull.*, vol. 66, Jun. 2020, doi: 10.1016/j.scib.2020.06.036.
- [142] X. Wang *et al.*, “Two facile routes to an AB&Cu-MOF composite with improved hydrogen evolution reaction,” *J. Alloys Compd.*, vol. 753, pp. 228–233, 2018, doi: <https://doi.org/10.1016/j.jallcom.2018.04.220>.
- [143] Y. Yang, P. Shukla, S. Wang, V. Rudolph, X.-M. Chen, and Z. Zhu, “Significant improvement of surface area and CO₂ adsorption of Cu–BTC via solvent exchange activation,” *RSC Adv.*, vol. 3, no. 38, pp. 17065–17072, 2013, doi: 10.1039/C3RA42519C.
- [144] M. Alfe, V. Gargiulo, L. Lisi, and R. Capua, “Synthesis and characterization of conductive copper-based metal-organic framework/graphene-like composites,” *Mater. Chem. Phys.*, vol. 147, pp. 744–750, Oct. 2014, doi: 10.1016/j.matchemphys.2014.06.015.